PTEN plays a role in the suppression of lateral pseudopod formation during *Dictyostelium* motility and chemotaxis

Deborah Wessels, Daniel F. Lusche, Spencer Kuhl, Paul Heid and David R. Soll*

W. M. Keck Dynamic Image Analysis Facility, Department of Biological Sciences, The University of Iowa, Iowa City, IA 52242, USA

*Author for correspondence (e-mail: david-soll@uiowa.edu)

Accepted 17 May 2007
Journal of Cell Science 120, 2517-2531 Published by The Company of Biologists 2007
doi:10.1242/jcs.010876

Summary

It has been suggested that the phosphatydylinositol (3,4,5)-trisphosphate [PtdIns(3,4,5)P_3] phosphatase and tensin homolog PTEN plays a fundamental role in *Dictyostelium discoideum* chemotaxis. To identify that role, the behavior of a *pten*$^-$ mutant was quantitatively analyzed using two-dimensional and three-dimensional computer-assisted methods. *pten*$^-$ cells were capable of polarizing and translocating in the absence of attractant, and sensing and responding to spatial gradients, temporal gradients and natural waves of attractant. However, all of these responses were compromised (i.e. less efficient) because of the fundamental incapacity of *pten*$^-$ cells to suppress lateral pseudopod formation and turning. This defect was equally manifested in the absence, as well as presence, of attractant. PTEN, which is constitutively localized in the cortex of polarized cells, was found essential for the attractant-stimulated increase in cortical myosin II and F-actin that is responsible for the increased suppression of pseudopods during chemotaxis. PTEN, therefore, plays a fundamental role in the suppression of lateral pseudopod formation, a process essential for the efficiency of locomotion and chemotaxis, but not in directional sensing.

Supplementary material available online at
http://jcs.biologists.org/cgi/content/full/120/15/2517/DC1

Key words: Motion analysis, Chemotaxis, Motility, Myosin II localization, F-actin localization, Myosin II dephosphorylation mutant 3XASP, PTEN, *Dictyostelium*

Introduction

In the process of chemotaxis, animal cells sense gradients of attractant and adjust direction accordingly. In *Dictyostelium discoideum*, phosphatidylinositol (3,4,5)-trisphosphate [PtdIns(3,4,5)P_3] has been implicated in this process (Zhou et al., 1998; Chen et al., 2003; Dormann et al., 2004; Franca-Koh et al., 2007). Upon stimulation by the chemoattractant cAMP, the PtdIns(3,4,5)P_3-binding proteins CRAC and AKT/PKB translocate to the leading edge of polarized cells (Parent and Devreotes, 1999; Meili et al., 1999; Servant et al., 2000; Haugh et al., 2000; Funamoto et al., 2001; Huang et al., 2003). The kinases responsible for PtdIns(3,4,5)P_3 synthesis, the phosphoinositide 3-kinases (PI 3-kinases), localize to the anterior pseudopod (Funamoto et al., 2002) and the phosphatase believed responsible for PtdIns(3,4,5)P_3 dephosphorylation, the tumor suppressor protein PTEN, localizes to the cortex of the posterior cell body (Funamoto et al., 2002; Iijima and Devreotes, 2002). These and other observations led initially to the hypothesis that a shallow extracellular spatial gradient of chemoattractant was amplified intracellularly through the genesis of a steep PtdIns(3,4,5)P_3 gradient, which in turn dictated cell polarity, anterior pseudopod extension and the direction of cellular translocation in an increasing spatial gradient of attractant (Funamoto et al., 2002; Iijima and Devreotes, 2002). Defects in the behavior of *pten*$^-$ and *pi(3)k1/2*$^-$ cells seemed consistent with this hypothesis (Funamoto et al., 2001; Iijima and Devreotes, 2002; Huang et al., 2003). Subsequently, it was proposed that PTEN and the PI 3-kinases must play roles downstream of the gradient sensing device (Devreotes and Janetopoulos, 2003; Franca-Koh et al., 2007). A number of observations were consistent with this latter hypothesis. First, Iijima and Devreotes (Iijima and Devreotes, 2002) reported that *pten*$^-$ cells challenged with a spatial gradient of attractant released from a micropipette ultimately did undergo chemotaxis, although with aberrant behavior (Iijima and Devreotes, 2002). Second, Andrew and Insall (Andrew and Insall, 2007) found that inhibition of PI 3-kinase activity with LY297002 did not affect the accuracy of chemotaxis in a spatial gradient of attractant, although pseudopod extension was aberrant. Third, Hoeller and Kay (Hoeller and Kay, 2007) deleted the five type I PI 3-kinases and PTEN from *D. discoideum* and observed that the sextuple mutant underwent chemotaxis in a spatial gradient of attractant, although again with aberrant behavior. These observations were consistent with an earlier report that the double mutant *pi(3)k1/2*$^-$ underwent chemotaxis in a spatial gradient of cAMP (Buczynski et al., 1997), although this result was later retracted (Funamoto et al., 2001). Third, it was found that attractant-stimulated relocalization of PtdIns(3,4,5)P_3-binding proteins from the cytoplasm to the membrane of the anterior pseudopod was not essential for chemotaxis (Postma et al., 2003; Postma et al., 2004). Finally, several studies in higher eukaryotes revealed that PTEN was not essential for chemotaxis (Lacalle et al., 2004; Nishio et al., 2007; Ferguson et al., 2007; Subramanian et al., 2007). But the exact role of PTEN remained elusive.

To explore that role, we have performed a high resolution computer-assisted analysis (Soll, 1995; Soll and Voss, 1998; Wessels and Soll, 1998; Wessels et al., 1998) of the behavior of *pten*⁻ cells of *D. discoideum*. Our results reveal that *pten*⁻ cells are able to polarize and translocate in the absence of attractant, and to sense and respond to spatial gradients, temporal gradients, and natural waves of attractant. But both in buffer and in spatial and temporal gradients of attractant, the response is compromised (i.e. less efficient), because *pten*⁻ cells are defective in suppressing lateral pseudopod formation. This defect results in unwarranted turning. Results are presented that further indicate PTEN is essential for the relocalization of myosin II and F-actin to the cortex, which is necessary for the suppression of lateral pseudopod formation.

Results

pten⁻ cells exhibit a behavioral defect in the absence of attractant

In previous studies, the behavior of *pten*⁻ cells had not been compared to that of parental cells in the absence of attractant, to test whether PTEN played a role in basic cell motility. To test this possibility, cells developed either in suspension by pulsing with cAMP, or on pads, were distributed at low density on the glass surface of a chamber and perfused with buffer in the absence of attractant. The majority of *pten*⁻ cells like parental AX2 cells were polar and motile (defined as migrated with average instantaneous velocities of above 3 μm per minute), but migration of *pten*⁻ cells was impaired (Table 1). The velocity of *pten*⁻ cell was reduced by approximately one half, and 'positive flow', a measure of area displacement (Soll, 1995), was reduced by approximately one-third (Table 1). In the absence of chemoattractant, *pten*⁻ cells moved less persistently than AX2 cells, as was evident in the 2D parameters reflecting persistence (e.g. directional change and directional persistence; Table 1) and in comparisons of 2D centroid and perimeter tracks (Fig. 1A-D). Cells of the rescued *pten*⁻ strain PTEN-GFP/*pten*⁻ regained the characteristics of the parent AX2 strain (data not shown).

Lateral pseudopod formation

The possibility that the decrease in persistence of *pten*⁻ cells could be the result of abnormally high frequencies of lateral pseudopod formation was tested by measuring the frequency and position of lateral pseudopod formation in two dimensions. A lateral pseudopod was defined in two dimensions as a protrusion extending at an angle ⩾30° from the anterior-posterior axis that attained an area ⩾15% of the total area of the cell body and did not arise by bifurcation or biased expansion of the original anterior pseudopod (Wessels et al., 1988). In the absence of attractant, *pten*⁻ cells formed lateral pseudopods at a frequency approximately 40% higher than that of parental cells (Table 2). The increase was due primarily to a four-fold increase in the frequency of pseudopod formation in the posterior half of a *pten*⁻ cell (Table 2). A qualitative analysis of lateral pseudopod formation by PTEN-GFP/*pten*⁻ cells revealed a return to the pattern of AX2 cells (data not shown).

The defect in the suppression of lateral pseudopod formation by *pten*⁻ cells (Table 2) was evident in 3D-DIAS reconstructions of living cells perfused with buffer. Like AX2 cells, *pten*⁻ cells were on average elongate, with their long axis extended on the substratum (Fig. 1F). A tapered uropod with tail fibers (color-coded green) was usually discernable. Multiple pseudopods, however, abnormally extended from both the anterior and posterior regions of *pten*⁻ cell (Fig. 1F). These pseudopods could become unusually long, flaccid and in some cases, ribbon-like (Fig. 1F). Frequently, one of these pseudopods wrapped around the *pten*⁻ cell body (Fig. 1F: 115 to 125 seconds), a behavior never observed in AX2 cells. Although the time it took for a lateral pseudopod to achieve maximum volume was similar between AX2 and *pten*⁻ cells, the rate of expansion of pseudopods of *pten*⁻ cells was approximately half that of AX2 cells (Table 3). Similarly, the maximum volume achieved by expanding *pten*⁻ pseudopods was less than half that of AX2 pseudopods (Table 3). The rates and total time of pseudopod retraction, however, were similar (Table 3). The differences observed in 3D reconstructions between the AX2 and *pten*⁻ cell in Fig. 1E and F, respectively, were representative of ten additional cells of each strain. A dynamic comparison of a representative AX2 and *pten*⁻ cell is presented in 3D in Movie 1 in supplementary material.

In the majority of experiments described here, cells were separated by two cell lengths (~30 μm) on average, and perfused at rates that turned over chamber volume four times per minute. To be sure that the differences between AX2 and

Table 1. *pten*⁻ cells migrating in buffer in the absence of chemoattractant exhibit reductions in velocity and persistence

Developmental condition	Strain	Number cells	Instantaneous velocity (μm/min)	Directional persistence (net/total dist.)	Directional change (deg./4 sec)	Positive flow (%/4 sec)	Maximum length (μm)	Maximum width (μm)	Area (μm^3)	% motile cells†
Pulsed with cAMP*	AX2	31	7.4±2.6	0.39±0.17	39.8±10.5	12.7±4.3	20.1±3.1	8.7±2.1	82±23	88
	pten⁻	46	4.6±1.4	0.18±0.16	66.0±16.2	9.0±1.8	19.7±4.3	8.5±1.9	88±23	77
	P value‡		10^{-7}	2×10^{-7}	4×10^{-13}	5×10^{-6}	NS	NS	2×10^{-2}	
Development on pads*	AX2	23	10.8±2.5	0.45±0.20	25.7±5.8	13.1±6.0	17.7±3.0	8.5±1.2	80±19	89
	pten⁻	27	4.7±1.6	0.13±0.11	47.9±5.8	6.8±1.7	16.0±4.1	7.8±1.6	79±22	72
	P value‡		7×10^{-12}	10^{-7}	10^{-17}	5×10^{-5}	NS	NS	NS	

Cells were perfused with buffer to prohibit them from conditioning their microenvironment through release of cAMP. Values are presented as mean ± standard deviation.

*To obtain aggregation-competent cells, development was driven either by pulsing cells in suspension with cAMP, or by allowing cells to signal naturally in dense cell carpets on filter pads saturated with buffer. In the latter case, the onset of aggregation in parental AX2 cell carpets began after 7 hours whereas that of *pten*⁻ cells began after 14 hours.

†A motile cell was one with an average instantaneous velocity over the period of analysis (5-10 minutes) of ⩾3 μm/minute. All parameters were computed for these motile cells.

‡The *P* values were considered significant if $P<0.05$ (Student's *t*-test); NS, not significant.

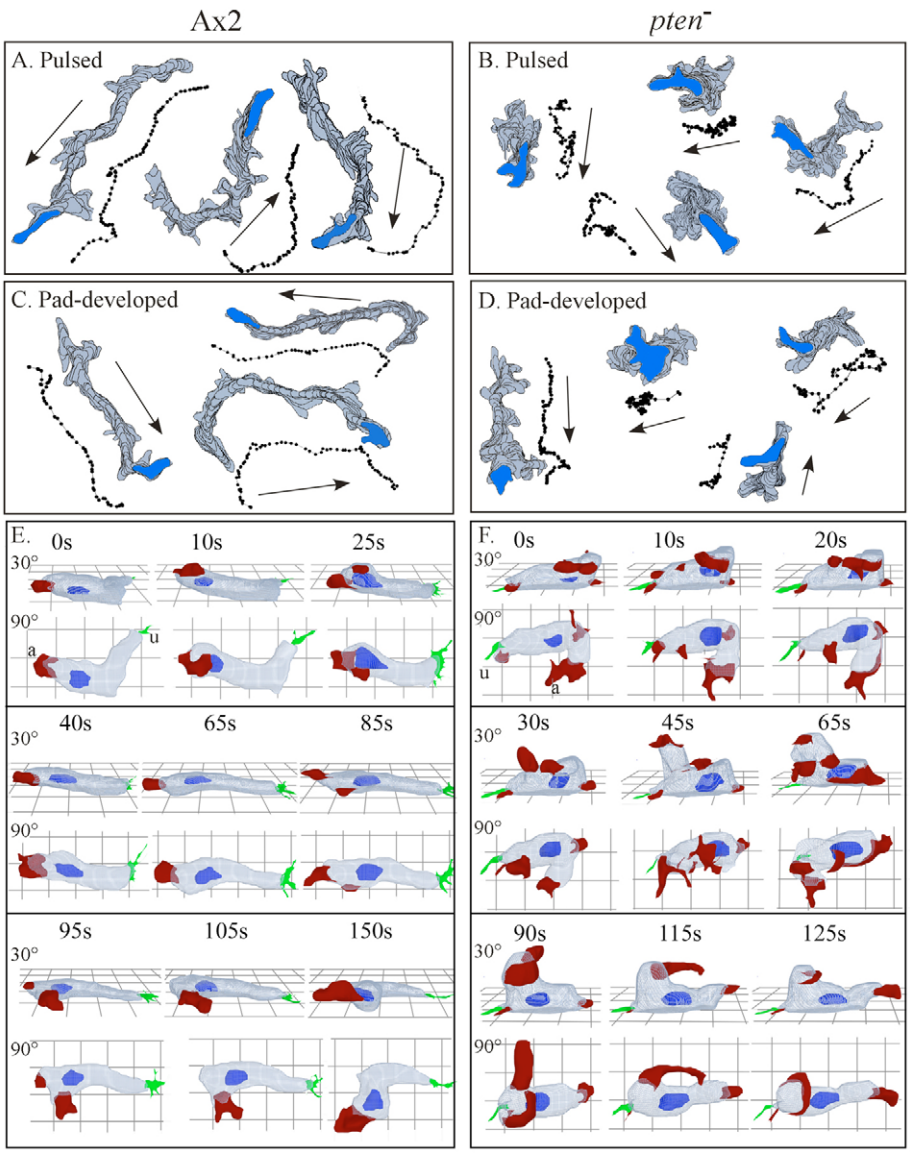

Fig. 1. *pten*⁻ cells exhibit fundamental defects in basic motile behavior and pseudopod formation in the absence of chemoattractant. Cells were distributed on the glass wall of a perfusion chamber at low density and perfused with buffer at a rate that turned over chamber volume four times a minute. (A,B) Perimeter and centroid tracks of representative parental AX2 (A) and *pten*⁻ (B) cells that had been pulsed for 6 hours with cAMP to achieve aggregation competence prior to motion analysis. (C,D) Perimeter and centroid tracks of representative AX2 (C) and *pten*⁻ (D) cells developed on pads to achieve aggregation competence prior to motion analysis. (E,F) Representative pad-developed parental AX2 (E) and *pten*⁻ (F) cell reconstructed in 3D with 3D-DIAS software over a 150 second or 125 second period, respectively, of cells migrating in buffer in a perfusion chamber. The arrows in A to D indicate net direction of cell migration. In E and F, pseudopods are colored red, the nucleus dark blue, tail fibers green and the cell body is shown in a transparent blue wireframe. Two views of the reconstructions are provided, at 30° and 90° angles. Note in F the abnormal extension of multiple lateral pseudopods by *pten*⁻ cells from the posterior as well as anterior end of the cell. See Movie 1 in supplementary material for a 3D dynamic presentation of an AX2 and *pten*⁻ cell migrating in buffer.

pten⁻ were for cells truly migrating in the absence of attractant, we repeated the perfusion experiments at very low cell densities (i.e. at distances between cells averaging 10 cell diameters, ~150 μm) and extremely high perfusion rates (i.e. at rates at which volume turned over six times a minute). Cells were analyzed only at the intake port with no upstream cells evident. The same differences between AX2 and *pten*⁻ cells were observed (data not shown).

pten⁻ cells break the rules for orderly pseudopod formation

As previously demonstrated (Wessels et al., 1996), wild-type cells translocating in the absence of attractant extend only one pseudopod at a time (Fig. 2A,B). This rule was broken by *pten*⁻ cells (Fig. 2C,D). *pten*⁻ cells extended multiple lateral pseudopods in parallel (Fig. 2C,D). Many of these pseudopods never achieved the average volume of AX2 pseudopods. Three additional AX2 cells and three additional *pten*⁻ cells were analyzed in 3D, with similar results. Reconstructions of PTEN-GFP/*pten*⁻ cells revealed a return to normal 3D pseudopod dynamics (data not shown).

pten⁻ cells undergo chemotaxis, but inefficiently

We next tested whether the specific behavioral defect exhibited by *pten*⁻ cells in buffer was manifested during chemotaxis in a spatial gradient of attractant. A majority of pulsed and pad-developed *pten*⁻ cells underwent chemotaxis in spatial gradients of cAMP (78 and 77%, respectively; Table 4), but centroid and perimeter tracks were more contracted, less directional, and less persistent (Fig. 3B,D) than those of AX2 cells (Fig. 3A,C). Pulsed- and pad-developed *pten*⁻ cells exhibited average chemotactic indices (CIs) of +0.18±0.25 and +0.28±0.29, respectively, less than half that of AX2 cells (Table 4). Histograms of chemotactic indices revealed that although a majority of *pten*⁻ cells, like AX2 cells, underwent chemotaxis in a spatial gradient of cAMP, *pten*⁻ cells could not achieve the high-end chemotactic indices that AX2 cells achieved (Fig. 4). Qualitative analyses of the tracks of cells of

Table 2. *pten*⁻ cells are defective in suppressing lateral pseudopod formation most notably along the posterior half of the cell body

A. Pseudopod formation in buffer and in spatial gradients of chemoattractant

Condition	Strain	Number of cells	Total lateral pseudopods/ 10 minutes	Lateral pseudopods, anterior half/ 10 minutes	Lateral pseudopods, posterior half/ 10 minutes
Buffer (B)	AX2	8	6.0±1.1	5.0±1.1	1.0±0.5
	pten⁻	9	8.6±1.8	4.6±0.7	3.9±1.7
	P value*		0.00323	0.46876	0.00071
Spatial gradient (SG)	AX2	20	1.6±2.0	1.5±1.7	0.2±0.4
	pten⁻	8	5.5±1.7	3.5±1.2	2.0±0.9
	P value*		0.00011	0.00248	0.0006

B. Ratios of the frequency of lateral pseudopod formation

	Anterior half	Posterior half	Anterior vs posterior
pten⁻ (B)/AX2 (B)	0.92	3.90	
pten⁻ (SG)/AX2 (SG)	2.33	10.00	
pten⁻ (B)/*pten*⁻ (SG)	1.31	1.97	
AX2 (B)/AX2 (SG)	3.33	5.00	
AX2 (B, Ant.)/AX2 (B, Post.)	–	–	5.00
pten⁻ (B, Ant.)/*pten*⁻ (B, Post.)	–	–	1.18
AX2 (SG, Ant.)/AX2 (SG, Post.)	–	–	7.50
pten⁻ (SG, Ant.)/*pten*⁻ (SG, Post.)	–	–	1.75

Values are presented as mean ± standard deviation.
*The *P* values were considered significant if $P<0.05$ (Student's *t*-test).

Table 3. The rate of lateral pseudopod extension is reduced in *pten*⁻ cells migrating in the absence of attractant

Strain	Number of cells	Rate of expansion (μm^3/5 seconds)	Time to maximum volume (seconds)	Maximum expansion volume (μm^3)	Rate of retraction (μm/5 seconds)	Time of retraction (seconds)
AX2	13	15±6	34±16	69±53	1.2±0.6	58±28
pten⁻	18	7±3	28±25	22±16	0.8±0.6	34±27
P value*		4×10^{-4}	NS	8×10^{-3}	NS	NS

The values are presented as mean ± standard deviation. All parameters were assessed with 3D-DIAS software (Heid et al., 2002; Wessels et al., 2006).
*The *P* values were considered significant if $P<0.05$ (Student's *t*-test).

the *pten*⁻ rescued strain PTEN-GFP/*pten*⁻ revealed a return to highly efficient chemotaxis (data not shown).

Lateral pseudopod formation in a spatial gradient of cAMP

pten⁻ cells undergoing chemotaxis in a spatial gradient of chemoattractant exhibited a decrease in average instantaneous velocity, a decrease in average directional persistence and an increase in average directional change when compared to AX2 cells (Table 4). These differences were similar to those in buffer (Table 1), suggesting that as in buffer, the main defect might be the incapacity to suppress lateral pseudopod formation. This proved to be the case (Table 2). The frequency of lateral pseudopod formation of *pten*⁻ cells was 3.4 times higher than that of for AX2 cells in a spatial gradient of cAMP (Table 2). The frequency in the posterior half of a *pten*⁻ cell was on average ten times higher than that of AX2 cells (Table 2). The defect was apparent in 3D reconstructions (Fig. 3E,F). A similar abnormality in pseudopod formation was suggested in earlier qualitative observations by Iijima and Devreotes (Iijima and Devreotes, 2002).

The response to temporal gradients of cAMP

During natural aggregation, *D. discoideum* amoebae respond to the temporal as well as spatial information in relayed waves of attractant (Varnum et al., 1985; Varnum-Finney et al., 1987a; Varnum-Finney et al., 1987b; Wessels et al., 1992; Soll et al., 2002). The responsiveness of a cell to the temporal information of a wave can be tested in a perfusion chamber in which increasing and decreasing concentrations of attractant are generated in sequence so that they mimic the concentrations and temporal dynamics of natural waves (Fig. 5) (Varnum et al., 1985; Varnum-Finney et al., 1987a; Wessels et al., 1992). *pten*⁻ cells (Fig. 5A,B), like AX2 cells (Fig. 5C,D), exhibited velocity increases in a majority of the front of the last three in a series of four temporal waves. The average magnitude of the surges of *pten*⁻ cells, however, was lower than that of AX2 cells (compare Fig. 5A with B), suggesting that *pten*⁻ cells failed to suppress lateral pseudopod formation in response to the increasing gradient in the front of each wave. An analysis of lateral pseudopod formation in two dimensions confirmed this prediction. While AX2 cells formed lateral pseudopods during the mid 2.5 minutes in the front of waves 2, 3 and 4 at an average frequency of 1.8±0.9 per 2.5 minutes (n=15 wave fronts), *pten*⁻ cells formed them at an average frequency of 3.5±1.0 per 2.5 minutes (n=15 wave fronts; $P<0.0001$).

Response to natural waves

The preceding results suggested that *pten*⁻ cells should be able to assess both the spatial and temporal information in natural

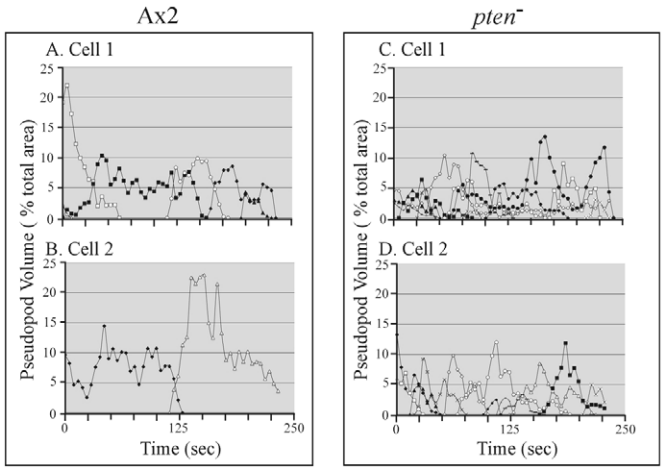

Fig. 2. *pten*⁻ cells abnormally extend multiple pseudopods at the same time. Different symbols represent different pseudopods. (A,B) The orderly extension of pseudopods by two representative parental AX2 cells. Note that only one pseudopod expands at a time, and that a previous pseudopod usually retracts when a new pseudopod expands. (C,D) The overlapping expansion of multiple pseudopods by two representative *pten*⁻ cells. Both anterior and lateral pseudopods were reconstructed and volumes estimated at each time point using 3D-DIAS software (Wessels et al., 1998; Heid et al., 2005).

waves of cAMP and respond by surging in the general direction of the source in the front of each wave, but that the response should be compromised because of the defect in lateral pseudopod suppression. To test this prediction, *pten*⁻ cells were vitally stained with DiI, mixed with majority unlabeled AX2 cells at a ratio of one to nine, respectively, and monitored for their response to waves generated by majority AX2 cells in submerged aggregation cultures (Escalante et al., 1997). Minority *pten*⁻ cells moved in surges in the general direction of the aggregation centers (Fig. 6A, red tracks), as did majority AX2 cells (Fig. 6A, black track). However, the paths were more erratic than those of AX2 cells, with more sharp turns that took cells off track. The average interval time between velocity peaks for AX2 and *pten*⁻ cells, however, were similar. A 2D analysis of pseudopod formation revealed that during the velocity surges, *pten*⁻ cells formed lateral pseudopods at a frequency approximately three times that of AX2 cells (data not shown). In aggregation territories composed exclusively of *pten*⁻ cells, behavior was cyclic but as was the case in AX2 territories, the cell tracks were more erratic (Fig. 6E). These results indicate that *pten*⁻ cells are capable of gradient sensing and chemotaxis in natural waves of cAMP generated by AX2 cells and in self-generated waves, but are less efficient in their response in both cases because of a defect in the suppression of lateral pseudopod formation.

pten⁻ and 3XASP cells share behavioral defects

The computer-assisted 2D and 3D methods used here to analyze *pten*⁻ cells have also been applied to varying degrees to over 20 other *D. discoideum* mutants, allowing behavioral comparisons between *pten*⁻ and these mutants. The behavioral defects of *pten*⁻ cells were remarkably similar to those of a subset of seven of these mutants, most notably the myosin II heavy chain phosphorylation mutant 3XASP (Heid et al., 2004; Heid et al., 2005). 3XASP contains a myosin heavy chain that mimics a constitutively phosphorylated state and, therefore, cannot readily polymerize in the cell cortex (Egelhoff et al., 1993; Egelhoff et al., 1996; Levi et al., 2002). As was the case for *pten*⁻ cells (Fig. 1B,D; Fig. 3B,D), the perimeter tracks of 3XASP cells in buffer (Fig. 7B) or in a spatial gradient of cAMP (Fig. 7D) were more compressed than those of parental JH10 cells (Fig. 7A and C, respectively), and 3D-DIAS reconstructions revealed that 3XASP cells abnormally extended multiple pseudopods from both anterior and posterior regions of the cell body (Fig. 7F), in contrast to parental JH10 cells (Fig. 7E). The behavioral parameters of 3XASP cells also differed from those of parental JH10 cells in a manner highly similar to that of *pten*⁻ and AX2 cells (Fig. 7G).

Myosin II and F-actin relocalization

In 3XASP cells, neither myosin II nor F-actin relocalize to the cell cortex in response to the increasing temporal gradient of

Table 4. *pten*⁻ cells undergo chemotaxis in a spatial gradient of cAMP, but exhibit reductions in velocity and chemotactic efficiency (i.e. chemotactic index)

Developmental condition	Strain	Number cells	Instantaneous velocity (μm/minute)	Directional persistence (net/total dist.)	Directional change (deg./4 seconds)	Positive flow (%/4 seconds)	Maximum length (μm)	Maximum width (μm)	%with Area (μm^3)	%with motile cells†	Chemotactic index (CI)	% cells positive CI
Pulsed with cAMP*	AX2	28	8.5±1.8	0.51±0.17	42.6±9.1	8.4±2.1	20.7±5.2	7.0±1.7	90±21	90.6	+0.51±0.26	94
	pten⁻	46	5.0±1.3	0.31±0.20	48.1±13.8	7.7±1.8	16.0±4.0	8.8±1.9	84±29	75.4	+0.18±0.25	78
	P value‡		2.4×10^{-7}	5.8×10^{-5}	4×10^{-2}	NS	1.5×10^{-4}	1.4×10^{-4}	NS		4.4×10^{-6}	
Development on pads*	AX2	35	10.5±3.6	0.56±0.24	28.9±11.1	9.0±2.6	19.3±3.1	7.9±1.7	90±20	90.0	+0.63±0.30	92
	pten⁻	42	5.7±2.6	0.44±0.15	34.5±8.6	7.5±1.8	17.1±3.7	7.2±1.6	80±21	81.5	+0.28±0.29	77
	P value‡		3.9×10^{-7}	1.7×10^{-2}	3×10^{-2}	1.2×10^{-2}	2.1×10^{-2}	1.3×10^{-1}	NS		8.7×10^{-5}	

Cells were analyzed on the bridge of a gradient chamber fashioned after that of Zigmond (Zigmond, 1977). Only motile cells moving at velocities ⩾3 μm per minute were analyzed.

*To obtain aggregation-competent cells, development was driven either by pulsing cells in suspension with cAMP, or by allowing cells to signal naturally in dense cell carpets on filter pads saturated with buffer. In the latter case, the onset of aggregation in parental AX2 cell carpets began after 7 hours whereas that of *pten*⁻ cells began after 14 hours.

†A motile cell was one with an average instantaneous velocity over the period of analysis (5-10 minutes) of ⩾3 μm/minute. All parameters were computed for these motile cells.

‡The Student's *t*-test was employed to compute the *P* value. The difference in values was considered significant if the $P<0.05$. $P>0.05$ was considered not significant (NS).

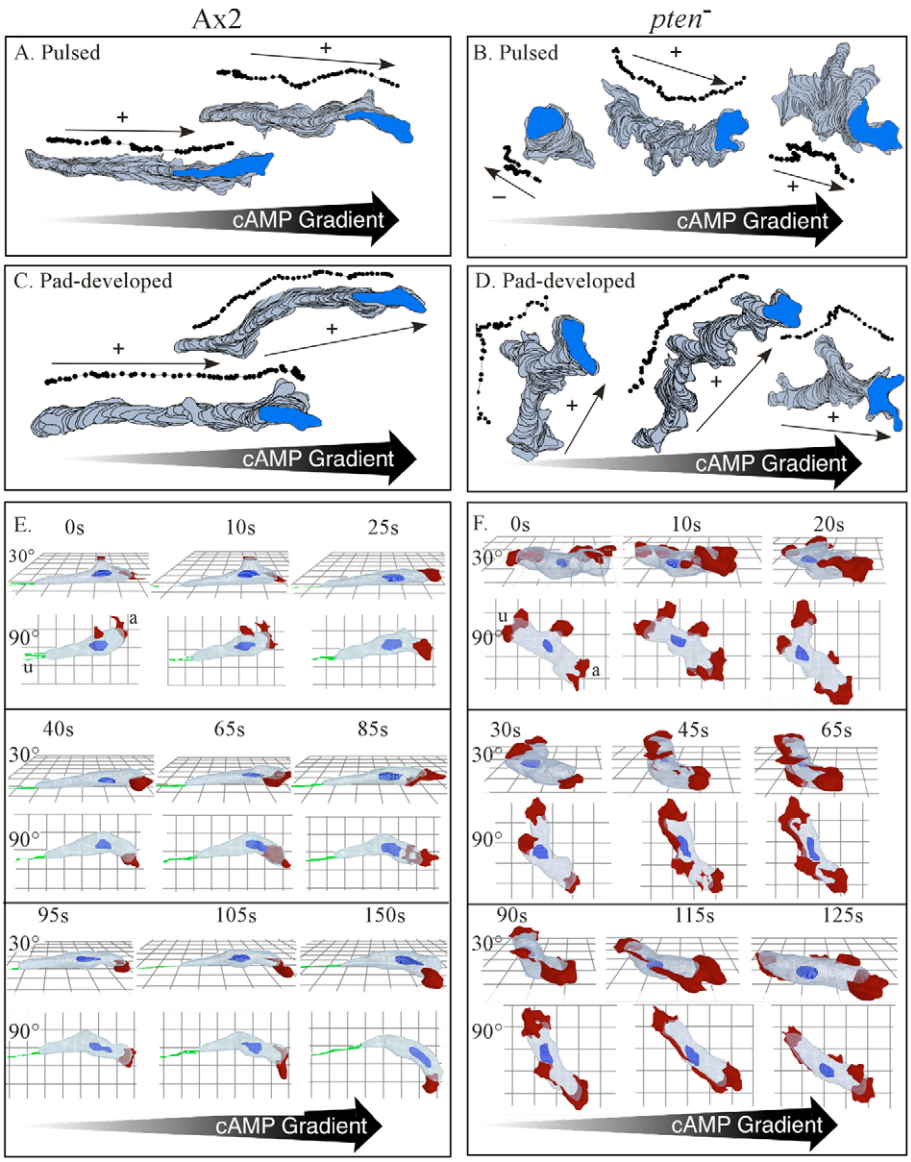

Fig. 3. Although *pten*⁻ cells undergo positive chemotaxis up spatial gradients of cAMP, they exhibit the same fundamental behavioral defects manifested in the absence of attractant. (A,B) Perimeter and centroid tracks of representative parental AX2 (A) and *pten*⁻ (B) cells pulsed for 6 hour with cAMP to achieve aggregation competence and then analyzed in a spatial gradient of attractant. (C,D) Perimeter and centroid tracks of representative parental AX2 (C) and *pten*⁻ (D) cells developed on pads to achieve aggregation competence and then analyzed in a spatial gradient of attractant. (E,F) Pad-developed parental (E) and *pten*⁻ (F) cells undergoing chemotaxis that were reconstructed with 3D-DIAS software over 150-second or 125-second periods, respectively. The thin arrows in A-D indicate the net direction of migration for each cell. The thick arrow in A-F indicates direction of increasing cAMP concentration. Plus (+) and minus (–) in A-D indicate a positive or negative chemotactic index, respectively, for each cell computed over the period of analysis. Color-coding of reconstructions in E and F are the same as in Fig. 1.

cAMP in the front of the third in a series of temporal waves, as they do in wild-type cells (Egelhoff et al., 1993; Egelhoff et al., 1996; Moores and Spudich, 1996; Levi et al., 2002; Laevsky and Knecht, 2003; Heid et al., 2004). A similar defect was observed in *pten*⁻ cells. For AX2 and *pten*⁻ cells migrating in the absence of attractant, myosin II was absent from pseudopods, and showed diffuse staining throughout the cytoplasm of the cell body, with only a hint of cortical localization (Fig. 8A,B and C,D, respectively). In the increasing temporal gradient of cAMP in the third in a series of temporal waves, there was an increase in myosin II in the cortex of AX2 cells (Fig. 8E,F), but not in the cortex of *pten*⁻ cells (Fig. 8G,H). Line scans of pixel intensity across the cell body supported this conclusion. Similar analyses of ten additional AX2 and *pten*⁻ cells provided similar results. Western analysis with anti-myosin II heavy chain antibody (Burns et al., 1995) demonstrated similar levels of total myosin II in parental AX2 and *pten*⁻ cells, both in buffer and in spatial gradients of cAMP (data not shown).

A similar analysis of F-actin localization was performed using Rhodamine-conjugated phalloidin staining. In both AX2 and *pten*⁻ cells migrating in buffer in the absence of attractant, F-actin localized intensely in pseudopods (Fig. 8I,J and K,L, respectively). There was diffuse, low intensity staining throughout the cytoplasm and a hint of cortical localization in both cell types. In an increasing temporal gradient in the front of the third in a series of four temporal waves, there was an increase in F-actin in the cortex of AX2 cells (Fig. 8M,N), but no comparable increase in *pten*⁻ cells (Fig. 8O,P). Line scans of pixel intensity supported this conclusion (Fig. 8M,N and O,P, respectively).

PTEN distribution

Since relocalization of both myosin II and F-actin in response to the increasing temporal gradient of attractant in the front of a wave requires PTEN, we compared the distribution of PTEN in response to attractant in an AX2 derivative that expressed PTEN-GFP. This strain behaved similarly to the parent AX2 strain in the absence of attractant, in response to a spatial gradient of attractant and in response to a temporal gradient of

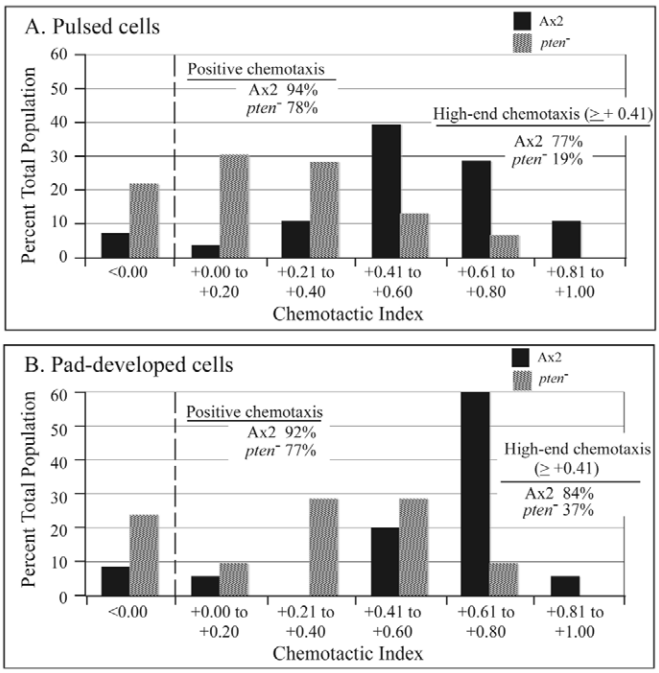

Fig. 4. Histograms of chemotactic indices (CI) demonstrate that the majority of *pten*⁻ cells undergo chemotaxis up a spatial gradient of cAMP, but do so with decreased efficiency. *pten*⁻ cells have difficulty achieving high-end CIs.

attractant (data not shown). In the absence of attractant, PTEN-GFP localized to the cortex of the main cell body and was found diffusely throughout the cytoplasm (Fig. 9A). Cortical localization ended at the junctions between the main cell body and both lateral and anterior pseudopods (Fig. 9A). No difference was observed between cells migrating in the absence of attractant (Fig. 9A) and cells undergoing chemotaxis in a spatial gradient of cAMP (Fig. 9B). The ratio of cortical to cytoplasmic staining were statistically indistinguishable, 1.9±0.27 for ten cells in buffer and 1.7±0.21 for ten cells in a spatial gradient of cAMP (P=0.16).

PTEN also localized to the cell cortex in the front (Fig. 9C), peak (Fig. 9D) and back (data not shown) of the third in a series of temporal waves of attractant. These results held true for ten cells analyzed similarly. Hence, whereas myosin II and F-actin increase in the cortex in response to attractant, PTEN remains constitutively localized in the cortex.

Discussion

PTEN, a potent tumor suppressor in vertebrates, has been implicated in cell migration and chemotaxis in both lower and higher eukaryotes (Sulis and Parsons, 2003). It possesses a phosphatase domain believed responsible for PtdIns(3,4,5)P_3 dephosphorylation and a C2-domain for membrane interactions (Lee et al., 1999; Vazquez et al., 2006; Cho and Stahelin, 2006). Its homology to tensin suggests a possible interaction with the cytoskeleton. In *D. discoideum*, it has been hypothesized that PTEN played a critical role in polarization and directed movement in the chemotactic response (Iijima and Devreotes, 2002; Funamoto et al., 2002; Iijima et al., 2004; Devreotes and Janetopoulos, 2003; Franca-Koh et al., 2007), but the exact role was not elucidated. Because 2D and 3D computer-assisted reconstruction and motion analysis of living cells provides a powerful tool for elucidating behavior defects in mutants and, hence, insights into the role of mutated proteins (Wessels and Soll, 1998; Soll et al., 2002), we used this approach on the *pten*⁻ mutant.

PTEN's role is constitutive

We show for the first time that PTEN plays a role in the suppression of lateral pseudopod formation in the absence, as well as in the presence, of attractant. When perfused with buffer, wild-type cells expressing PTEN form lateral pseudopods

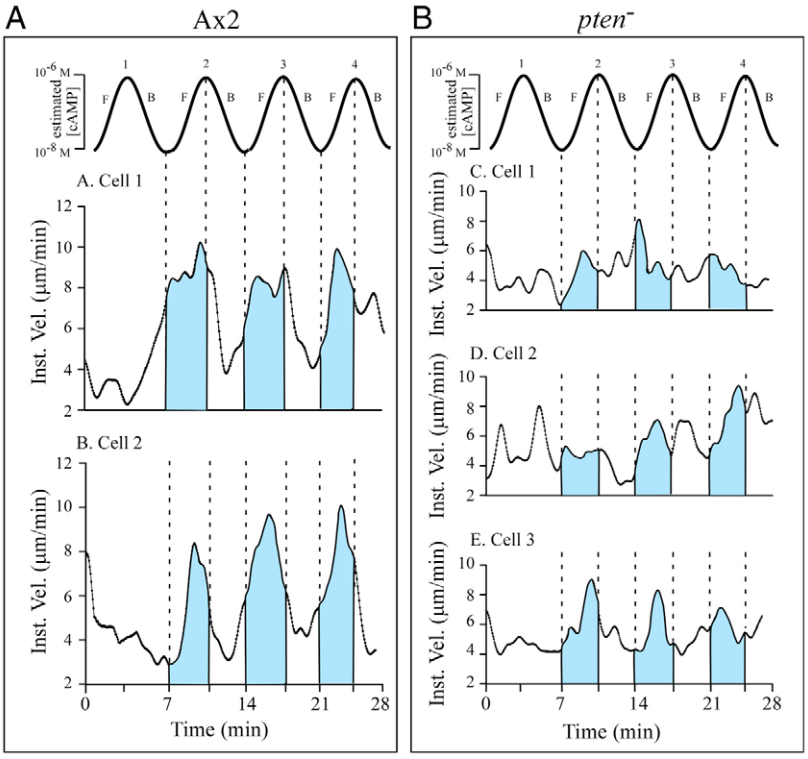

Fig. 5. *pten*⁻ cells respond to the increasing temporal gradient of cAMP in the last three of a series of four temporal waves generated in a perfusion chamber in the absence of established spatial gradients. These waves mimic the temporal dynamics of natural waves (Tomchik and Devreotes, 1981), but the response is lower than that of parental AX2 cells. (A) Time plots of the instantaneous velocity (Inst. Vel.) of two representative AX2 cells responding to four successive temporal waves of cAMP. AX2 cells exhibit an increase in velocity in the front of the last three of four successive temporal waves of attractant. They do not respond to the first wave, as previously reported (Varnum et al., 1985; Wessels et al., 1992). (B) The instantaneous velocity of three representative *pten*⁻ cells responding to four successive temporal waves of cAMP. *pten*⁻ cells exhibit, on average, an increase in velocity in the front of the last three waves, but the magnitude of the increase is far below that of AX2 cells. Behavior in the front of each wave is color-coded blue.

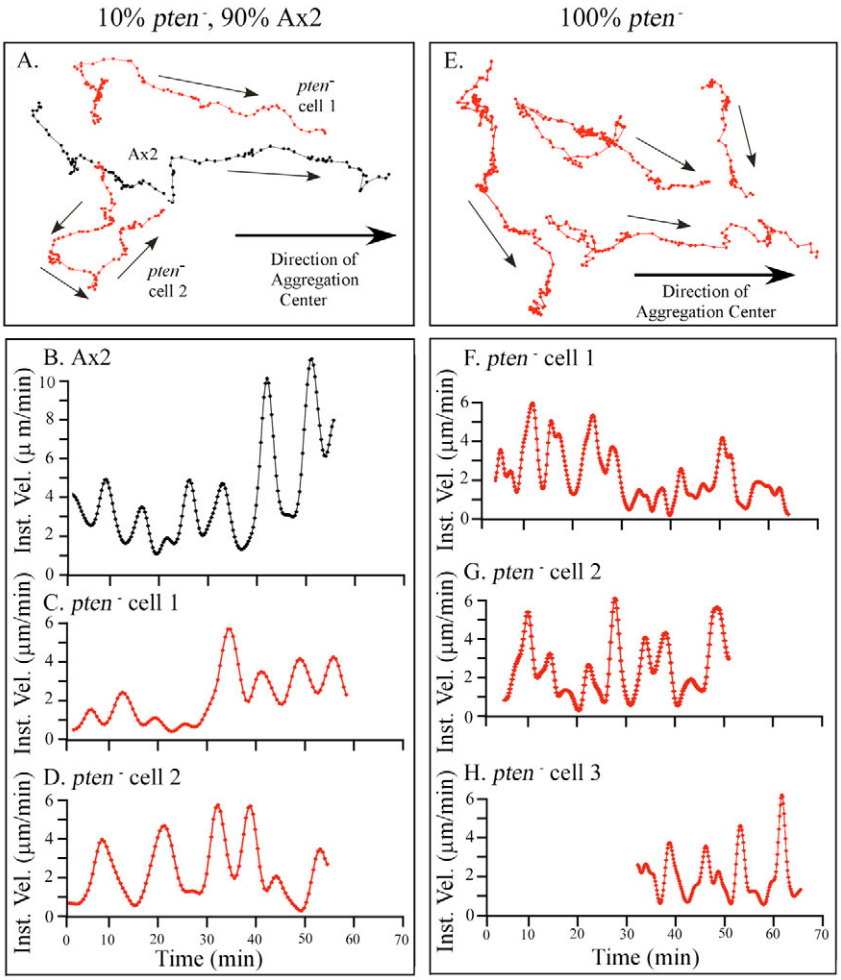

Fig. 6. *pten*⁻ cells undergo natural chemotaxis, but less efficiently than AX2 cells. (A) Selected centroid tracks of one representative AX2 and three representative *pten*⁻ cells undergoing chemotaxis in an aggregation territory made up of 90% AX2 and 10% *pten*⁻ cells in a submerged culture. (B-D) Velocity plots of one representative majority AX2 cell and two representative minority *pten*⁻ cells in a mixed aggregation territory made up of 90% AX2 cells and 10% *pten*⁻ cells. (E) Selected centroid tracks of four representative *pten*⁻ cells undergoing chemotaxis in an aggregation territory made up of 100% *pten*⁻ cells in a submerged culture. (F-H) Velocity plots of three representative *pten*⁻ cells in a homogeneous *pten*⁻ aggregation territory in a submerged culture. Small arrows in A and E indicate net direction.

on average every 2 minutes (Wessels et al., 2000a). Wild-type cells extend only one pseudopod at a time (Wessels et al., 2000a; Wessels et al., 1996) and rarely from the posterior half of the cells (Varnum-Finney et al., 1987b; Wessels et al., 2000a; Wessels et al., 2000a). When perfused with buffer, *pten*⁻ cells formed lateral pseudopods at a frequency approximately 50% higher than wild-type cells, extended them frequently from the posterior end and extended more than one at a time.

In a spatial or increasing temporal gradient of cAMP, the average frequency of lateral pseudopod formation of wild-type cells is reduced to once every 4-5 minutes (Kumar et al., 2004; Shutt et al., 1995; Stepanovic et al., 2005; Varnum-Finney et al., 1987a; Wessels et al., 2000a; Wessels et al., 2000b; Zhang et al., 2003). In marked contrast, *pten*⁻ cells challenged with spatial or temporal gradients of cAMP continued to form lateral pseudopods at abnormally high frequency, and continued to extend them in parallel and from the rear of the cell. Hence, PTEN plays a constitutive role in the suppression of lateral pseudopod formation.

In none of the chemotaxis assays performed here with *pten*⁻ cells was there an indication of a defect in the actual mechanism of gradient sensing or maintenance of polarity (i.e. in maintaining an anterior-posterior axis with defined uropod). *pten*⁻ cells were fully capable of interpreting the direction of a spatial gradient and moving in the general direction of increasing attractant concentration both in vitro and in the front of a natural wave. In both cases, however, translocation paths were more erratic because of unwarranted turns. Furthermore, whereas *pten*⁻ cells surged in an increasing temporal gradient in the front of a simulated temporal wave, the increase in velocity was dampened by unwarranted turns. Hence, although the responses to spatial and temporal gradients of attractant were intact, the efficiency of each response was diminished. Recently, Andrew and Insall (Andrew and Insall, 2007) demonstrated that in preparations in which cells were challenged with a spatial gradient of attractant, inhibition of PI 3-kinase activity with LY294002 affected the angle of pseudopod formation, but not direction (i.e. not gradient sensing). Hoeller and Kay (Hoeller and Kay, 2007) deleted all five PI 3-kinase genes as well as PTEN, and observed near-normal chemotaxis under the conditions employed. Moreover, a number of studies of animal cells demonstrated that PTEN-deficient cells underwent chemotaxis (Lacalle et al., 2004; Nishio et al., 2007; Ferguson et al., 2007; Subramanian et al., 2007). Together with our observations, these results call into question a role for an intracellular PtdIns(3,4,5)P_3 gradient in sensing an extracellular gradient of attractant or in the maintenance of cell polarity. Moreover, the constitutive role played by PTEN in pseudopod suppression demonstrated here calls into question the accuracy of models in which PTEN has

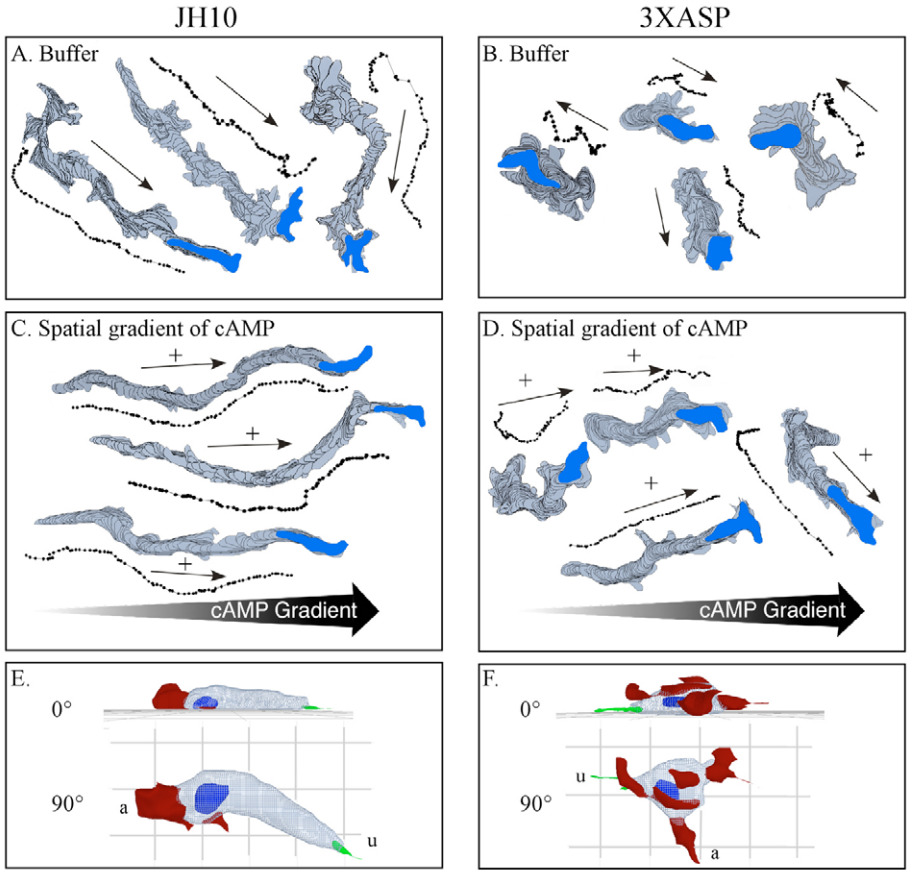

G. Similarity of behavioral defects between 3XASP and *pten*⁻

	In absence of cAMP			Spatial gradient of cAMP			
	Instant. vel.	Dir. change	Pers.	Instant. vel.	Dir. change	Chemotactic Index	% Pos. chemotaxis
3XASP/JH10	0.53	1.4	0.61	0.48	1.5	0.55	0.85
pten⁻ (pulsed)/Ax2	0.62	1.7	0.46	0.59	1.1	0.35	0.85
pten⁻ (pad-dev)/Ax2	0.44	1.9	0.28	0.54	1.0	0.44	0.89

Fig. 7. The defects in the behavior of cells of the myosin heavy chain phosphorylation mutant 3XASP in the absence of attractant and in a spatial gradient of cAMP are remarkably similar to those of *pten*⁻ cells. (A,B) Centroid and perimeter tracks of representative parental JH10 and representative 3XASP cells, respectively, migrating in buffer in a perfusion chamber in the absence of attractant. (Compare with data for corresponding *pten*⁻ cells in Fig. 1B,D.) (C,D) Centroid tracks and perimeter tracks of representative JH10 and 3XASP cells, respectively, undergoing chemotaxis in a spatial gradient of cAMP. Arrows in A-D indicate net direction and + signs in C and D indicate a positive chemotactic index. (Compare with corresponding *pten*⁻ data in Fig. 3B,D.) (E,F) 3D-DIAS reconstructions of a JH10 and 3XASP cell, respectively, translocating in buffer reveal that whereas the former extends a dominant anterior pseudopod with occasional lateral pseudopods, the latter extends multiple pseudopods from both anterior and posterior regions of the cell body. Color coding of reconstructions are the same as in Fig. 1. (Compare with corresponding data for AX2 and *pten*⁻ in Fig. 1E and F, respectively.) (G) The defects in motility and chemotaxis reflected in measured parameters are remarkably similar for 3XASP and *pten*⁻ cells. The ratio of the average mutant to parental parameter is presented for cells translocating in the absence of cAMP and for cells responding to a spatial gradient of cAMP. Instant. vel., instantaneous velocity; Dir. change, direction change; Pers., directional persistence; % Pos. chemotaxis, percentage positive chemotaxis. The 2D and 3D analyses of JH10 and 3XASP for A-F were performed anew for this study. The data for computing the parameter proportions for 3XASP and JH10 represent a combination from Heid et al. (Heid et al., 2004) and new experiments. The chemotactic index for 3XASP was recomputed from new data for which interval time was the same as that used for the *pten*⁻ study.

been placed as a downstream component of a regulatory pathway for chemotaxis that is activated by chemoattractant (Franca-Koh et al., 2007).

PTEN and the cortical localization of myosin II and F-actin

In reviewing the behavioral defects of more than fifteen *D. discoideum* mutants that have been subjected to computer-assisted methods, we identified a subset remarkably similar to *pten*⁻ cells. They included the null mutant of the myosin II heavy chain (MHC), *mhcA*⁻ (Wessels et al., 1989; Wessels and Soll, 1990; Peters et al., 1988; Sheldon and Knecht, 1996; Heid et al., 2004), the MHC dephosphorylation mutant, 3XASP (Heid et al., 2004), the null mutant of clathrin, *chc*⁻ (Wessels et al., 2000a), the null mutant for sphingosine-1-phosphate (S-1-P) lyase (Kumar et al., 2004), and null mutants of three class I myosins, *myoB*⁻, *myoA*⁻ and *myoF*⁻ (Falk et al., 2003; Titus et al., 1993; Wessels et al., 1996). The remaining mutants that were subjected to computer-assisted methods exhibited a variety of behavioral defects quite distinct from those of *pten*⁻ and this subset (Cox et al., 1992; Cox et al., 1996; Alexander et al., 1992; Shutt et al., 1995; Wessels et al., 2000a; Wessels et al., 2000b; Zhang et al., 2002; Bosgraaf et al., 2002; Bosgraaf et al., 2005; Stepanovic et al., 2005).

The MHC of 3XASP cannot readily polymerize and localize to the cell cortex (Egelhoff et al., 1993; Egelhoff et al., 1996). The spatial and temporal gradients of cAMP associated with the front of a natural wave do not, therefore, stimulate an increase in cortical myosin II or the associated increase in cortical F-actin in the 3XASP mutant (Yumura and Fukui, 1985; Yumura and Uyeda, 1997; Wessels et al., 2000b; Wessels et al., 2004; Zhang et al., 2002; Zhang et al., 2003; Heid et al.,

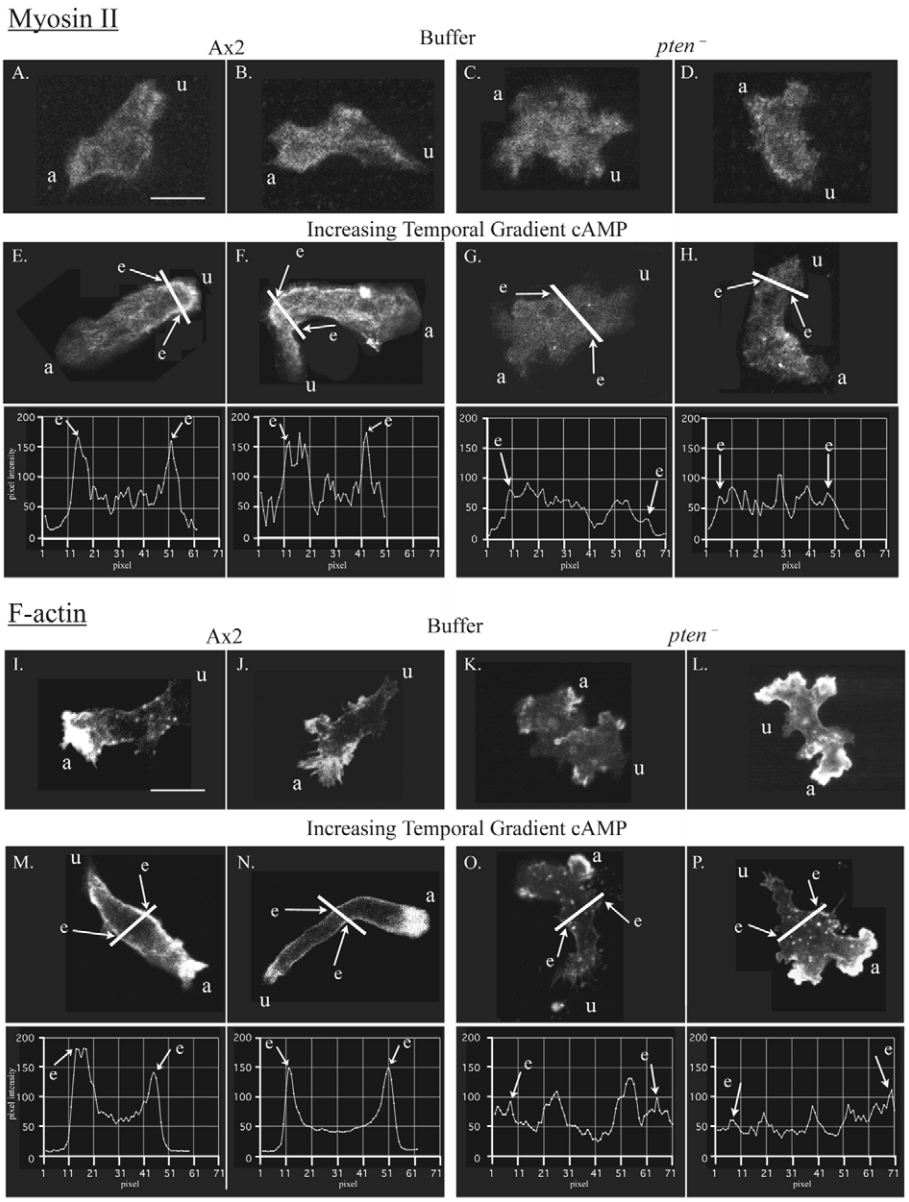

Fig. 8. *pten*⁻, like 3XASP, is defective in myosin II and F-actin localization to the cortex in response to an increasing temporal gradient of cAMP in the front of a temporal wave. (A,B and C,D) Indirect immunofluorescent staining of myosin II heavy chain in parental AX2 and *pten*⁻ cells, respectively, migrating in buffer in the absence of attractant. Note that in both cases, there is very little cortical localization of myosin II. (E,F and G,H) Indirect immunofluorescent staining of myosin II heavy chain and laser scanning confocal microscopic (LSCM) line scans of pixel intensity of AX2 cells and *pten*⁻ cells, respectively, migrating in the front of the third temporal cAMP wave in a series. Note that whereas there is a substantial increase in cortical staining in AX2 cells, there is no detectable increase in cortical staining in *pten*⁻ cells. (I,J and K,L) Phalloidin staining of F-actin in Ax2 and *pten*⁻ cells, respectively, migrating in buffer. Note that whereas the pseudopodia stain brightly for F-actin, there is only a hint of cortical staining in both cell types in buffer. (M,N and O,P) Phalloidin staining of F-actin and LSMC line scans of pixel intensity of AX2 cells and *pten*⁻ cells, respectively, in the third of a series of temporal waves of cAMP. Note that whereas there is a substantial increase in cortical staining in AX2 cells, there is no similar increase in *pten*⁻ cells. a, anterior end; u, uropod; e, cell edge. Line across cells in A-H, and M-P, indicates position of scan.

2004). Previously it was suggested that the cortical actin-myosin cytoskeleton acted as a barrier to lateral pseudopod formation (Wessels et al., 1988; Wessels and Soll, 1990; Spudich, 1989), and subsequent studies demonstrated that cortical myosin II polymerization generated cortical tension (Egelhoff et al., 1996; Lee et al., 1994; Lück-Vielmetter et al., 1990; Pasternak et al., 1989). Interestingly, the myosin I mutant *myoB*⁻, which exhibits behavioral defects similar to those of *pten*⁻ and 3XASP cells (Wessels et al., 1996), has also been shown to exhibit a decrease in cortical tension, suggesting a cooperative role with myosin II in generating cortical tension (Dai et al., 1999).

Previous experiments in which *pten*⁻ cells were globally stimulated by the rapid addition (i.e. within seconds) of a high concentration of attractant (10^{-6} M cAMP) revealed exaggerated F-actin polymerization (Iijima and Devreotes, 2002). Such global stimulation, however, is non-physiological since cells normally experience gradual rather than rapid changes in attractant in relayed waves during natural chemotaxis (Tomchik and Devreotes, 1981; Soll et al., 2002). Global stimulation by the rapid addition of 10^{-6} M cAMP has been demonstrated to cause a highly abnormal response that includes the immediate cessation of cellular translocation, an immediate decrease in cytoplasmic flow, a rapid loss of F-actin in pseudopodia, a rapid increase in cortical F-actin and a rapid, transient increase in total cell F-actin (Wessels et al., 1989; Varnum and Soll, 1984; Varnum et al., 1985; Varnum-Finney et al., 1988; Hall et al., 1988; Futrelle et al., 1981; Condeelis et al., 1988; Dharmwardhane et al., 1989; McRobbie and Newell, 1983; Chen et al., 2003). We therefore compared myosin II and F-actin localization between cells migrating in the absence of attractant and cells responding to the third in a series of temporal waves that mimicked the temporal dynamics of natural waves. As was the case for 3XASP cells, neither myosin II nor F-actin increased in the cortex of *pten*⁻ cells in response to an increasing temporal gradient of attractant

(Egelhoff et al., 1996; Zhang et al., 2002; Zhang et al., 2003; Wessels et al., 2000b; Wessels et al., 2004; Heid et al., 2004). Together, these results suggest that in response to the front of a natural wave of attractant, PTEN may be essential for the normal increase in cortical myosin II and F-actin, which functions to further suppress lateral pseudopod formation during chemotaxis, presumably through increased cortical tension.

Because PTEN exhibits homology to tensin (Lee et al., 1999; Li et al., 1997; Steck et al., 1997), we entertained the possibility that it could interact with the F-actin-myosin II cytoskeleton, perhaps entering the cortex in combination with F-actin and myosin II, in response to the increasing temporal and positive spatial gradients of attractant associated with the front of a wave. Previous experiments in which wild-type cells were globally stimulated by the rapid addition of a high concentration of cAMP (10^{-6} M) revealed a transient decrease in cortical PTEN (Funamoto et al., 2002; Iijima and Devreotes, 2002) that occurred at the expected time of transient pseudopod retraction, the cessation of cellular translocation, depolymerization of pseudopodial F-actin and doubling of total cell F-actin (Wessels et al., 1989). It is, therefore, difficult to ascribe a role for this transient decrease in cortical PTEN to cell locomotion or chemotaxis. It was also demonstrated that when attractant is released from a micropipette on one side of a latrunculin-treated cell, which is rendered apolar due to the depolymerization of F-actin, PI 3-kinase and phosphoinositide-3-binding proteins rapidly localize to the side of the cell that first experiences attractant, whereas PTEN localizes to the opposite side of the cell, indicating that a gradient of attractant can immediately and correctly polarize a 'naïve' cell, and induce PTEN localization away from the source of attractant (Janetopoulos et al., 2004). Here we have found, however, that once a cell is polarized, PTEN remains at the same level in the cortex in absence or presence of attractant. PTEN localizes similarly in the cortex of the posterior two-thirds of a cell oriented up a spatial gradient of attractant, a cell oriented at a 45° angle to a spatial gradient or even oriented in the wrong direction (i.e. down the gradient; D.W. and D.R.S., unpublished). It also localizes similarly in the front, peak and back of a temporal wave of cAMP that mimics the temporal dynamics of a natural wave. Hence, once polarity is established, the direction of the extracellular spatial or temporal gradient does not appear to affect the cortical localization of PTEN along the anterior-posterior cell axis. Although these observations are not consistent with cooperative relocalization of PTEN, F-actin and myosin II to the cell cortex in response to a chemotactic signal, such a mechanism cannot be ruled out given the dynamic fashion in which PTEN may interact with the plasma membrane (Vazquez et al., 2006).

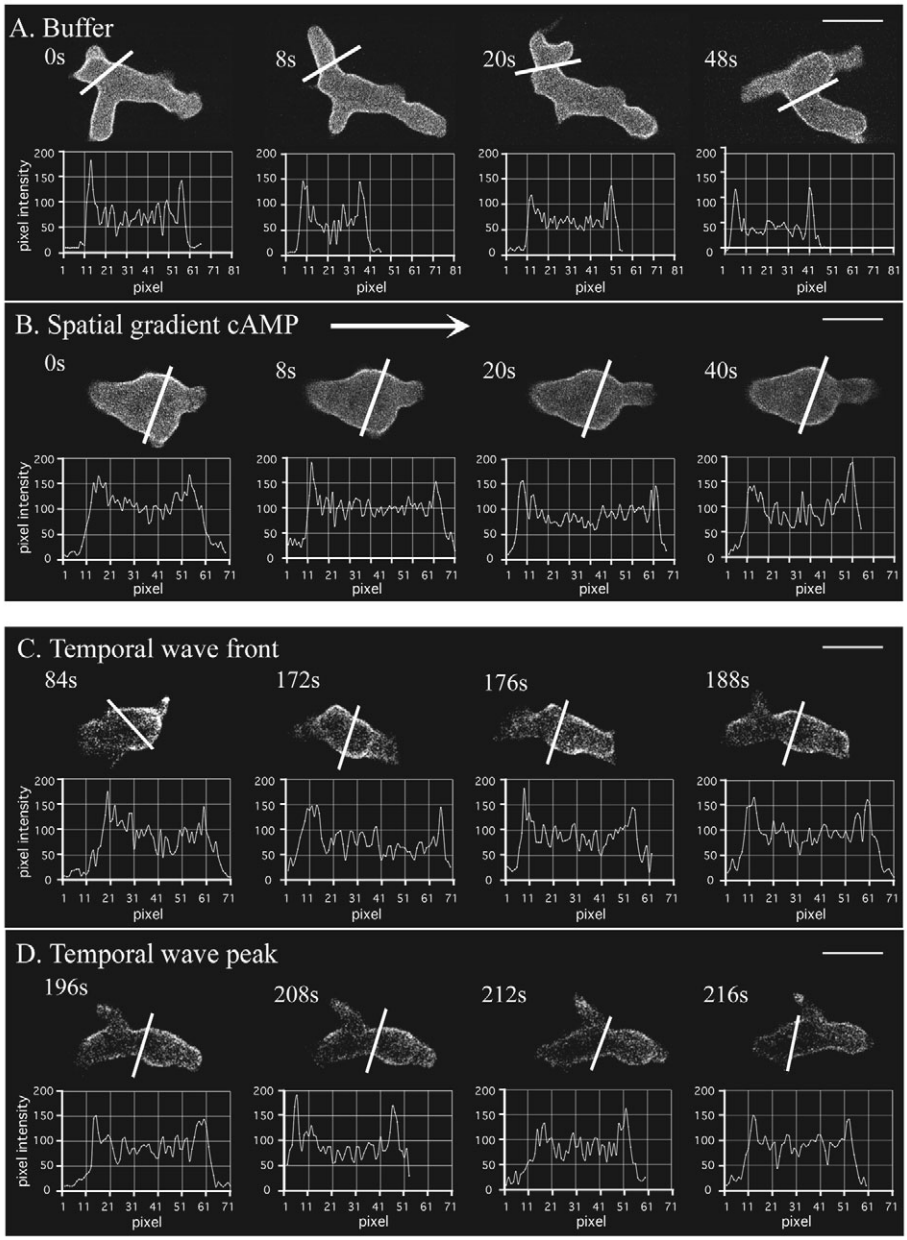

Fig. 9. PTEN is constitutively localized in the cortex. AX2 cells expressing GFP-PTEN were analyzed in buffer, in a spatial gradient of attractant and in the front of the third in a series of temporal waves of cAMP. (A) Perfused with buffer in a perfusion chamber in the absence of attractant. (B) Oriented up a spatial gradient of cAMP. (C,D) In the front and at the peak, respectively, of the third in a series of temporal waves of cAMP. LSCM line scans of pixel intensity are presented below each LSCM image, and the position of each line scan is indicated by a white line across each image. Note the similarity of peaks at cell edges under all conditions.

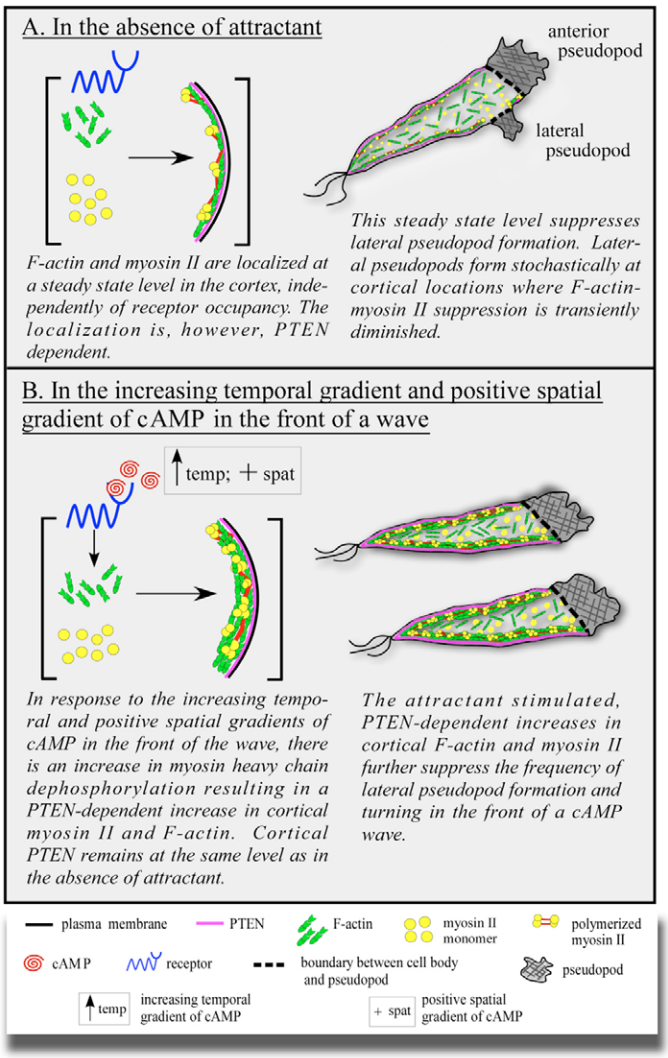

Fig. 10. A model for the role of PTEN in the suppression of lateral pseudopod formation. In the absence and in the presence of attractant, PTEN localizes constitutively at the same level in the cortex of the main cell body. (A) In the absence of attractant, a low steady state level of MHC-dephosphorylation results in myosin II and F-actin localization in the cortex with PTEN. This steady state localization is responsible for the suppression of lateral pseudopod formation through the generation of cortical tension. Once every 2 minutes in the absence of attractant, a lateral pseudopod forms randomly, usually from the anterior half of the cell body at a site where the myosin II-F-actin cortex transiently weakens. (B) In response to the increasing temporal and positive spatial gradients of attractant in the front of wave, a receptor-mediated signal transduction pathway is activated that increases the rate of myosin II dephosphorylation, resulting in an increase in cortical myosin II and F-actin. This results in an increase in cortical tension, leading to the increased suppression of lateral pseudopod formation in the front of a wave. In this model, receptor-mediated dephosphorylation of MHC is responsible for increased cortical tension. The similar behavioral defects of the mutants myoA, myoB, myoF, clathrin and sphingosine-1-phosphate lyase suggest that they also play roles in steady state pseudopod suppression in the absence of attractant and increased suppression in the front of a wave. In the model, PTEN is essential for myosin II-F-actin localization and pseudopod suppression in the absence of attractant, and the increases in localization and suppression in the front of the wave. But because it remains at a constitutive level in the cortex, it has not been placed in the receptor-activated transduction pathway leading to increased pseudopod suppression. It should be emphasized that this model deals with a mechanism that affects the efficiency of the chemotactic response through lateral pseudopod suppression, not with a mechanism of gradient sensing or the maintenance of cellular polarity.

A model for PTEN, myosin II and lateral pseudopod suppression

We have, therefore, presented evidence that the sole role of PTEN appears to be in the suppression of lateral pseudopod formation. We have shown for the first time that PTEN plays this role in the absence, as well as, in the presence of attractant. PTEN appears to function as a mediator of F-actin-myosin II localization in the cell cortex. In a model that accommodates these results (Fig. 10), we propose, first, that PTEN is essential for cortical localization of an F-actin-myosin II-based cytoskeleton that is responsible for the suppression of lateral pseudopod formation through the generation of cortical tension. In the absence of attractant, this system functions at steady state, resulting in a level of F-actin-myosin II localization in the cortex that allows lateral pseudopods to form spontaneously on average once every 2 minutes (Fig. 10A). Lateral pseudopods form stochastically at random sites primarily along the cortex of the anterior portion of the main cell body where the cortical cytoskeleton is transiently weakened or disrupted, and cortical tension transiently diminished (Postma et al., 2003). When cells orient and rapidly move in the direction of an aggregation center in response to the positive spatial gradient and increasing temporal gradient of attractant associated with the front of a natural wave, there is a receptor-mediated increase in the rate of myosin II heavy chain (MHC) dephosphorylation, resulting in increased cortical localization of the actin-myosin cytoskeleton, increased cortical tension, and further suppression of lateral pseudopods (Fig. 10B). The frequency of lateral pseudopod formation decreases to less than one every 5 minutes. The suppression of lateral pseudopod formation increases the efficiency of chemotaxis by keeping a correctly oriented cell on track (Soll et al., 2002). The common behavioral defects of *pten*$^-$, 3XASP, the deletion mutants of the three class I myosins, clathrin and S-1-P lyase, suggest that the steady state level of lateral pseudopod formation in the absence of attractant, and further suppression of lateral pseudopod formation in the front of a wave, involve proteins heretofore not considered in previous models for the role of PTEN in *D. discoideum* motility and chemotaxis.

Materials and Methods

Origin, maintenance and development of strains

Frozen stocks of the mutant *pten*$^-$, the rescue strain PTEN-GFP/*pten*$^-$ and the parental AX2, generously provided by Peter Devreotes, Johns Hopkins University (Iijima and Devreotes, 2002), were reconstituted every 3 weeks in HL-5 growth medium (Cocucci and Sussman, 1970) supplemented with 5 μg/ml of blasticidin in the case of *pten*$^-$ and PTEN-GFP/*pten*$^-$. Growth medium of the rescue strain also contained 10 μg/ml of G418. The myosin heavy chain phosphorylation mutant 3XASP and its parental strain JH10 (Egelhoff et al., 1993) were maintained as previously described (Heid et al., 2004).

Two different protocols were used to generate cAMP-responsive, motile cells. In the first, cells suspended in buffered salts solution (BSS: 20 mM KCl, 2.5 mM $MgCl_2$, 20 mM KH_2PO_4, 5 mM Na_2HPO_4, pH 6.4) at a density of 5×10^6 per ml were pulsed every 6 minutes with 50 nM cAMP for 6 hours at 22°C, as previously

described (Iijima and Devreotes, 2002; Wessels et al., 2004). In the second protocol, cells were developed on filter pads as previously described (Soll, 1979; Wessels et al., 2006).

Generation of a PTEN-GFP-expressing AX2 strain

The AX2-PTEN-GFP strain was generated according to protocols described by Sandman et al. (Sandman et al., 1997). In brief, AX2 cells were washed in ice-cold buffer supplemented with 50 mM sucrose, mixed with 5 μg of PTEN-pTX-GFP obtained from the *Dictyostelium* Stock Center (http://dictybase.org/StockCenter/StockCenter.html) and then electroporated with a Bio-Rad Electroporator at 3 μF and 1.7 kV. Clonal populations of G418-resistant transformants were obtained by Fluorescence Activated Cell Sorting (FACS) at the University of Iowa Flow Cytometry Facility.

Behavioral analysis

2D-DIAS (Two-dimensional Dynamic Image Analysis System) software was used to examine motility in the absence of attractant. A low density suspension of cells was distributed on a 25 mm glass coverslip in a Sykes-Moore perfusion chamber (Bellco Glass, Vineland, NJ) as described in detail elsewhere (Varnum et al., 1986). The chamber was perfused with BSS at a rate that turned over one chamber volume-equivalent every 15 seconds. A cell density was determined that allowed individual, uninterrupted cell migration over a 10-minute period.

2D-DIAS was also used to examine chemotaxis in a spatial gradient (Soll, 1995; Soll and Voss, 1998). Cells were dispersed on the bridge of a Plexiglas chamber (Varnum and Soll, 1984) designed after that of Zigmond (Zigmond, 1977). For 3D-DIAS studies (Soll and Voss, 1998; Wessels et al., 1998), cells were dispersed on the quartz bridge of a chamber suitable for optical sectioning with differential interference contrast (DIC) microscopy (Shutt et al., 1998). In both spatial gradient chambers, BSS alone was added to one of the two troughs bordering the bridge and BSS containing 10^{-6} M cAMP was added to the parallel trough.

For the analysis of cellular responses to temporal cAMP waves, the NE-1000 Multi-Phaser Programmable Syringe Pump (New Era Pump Systems, Wantagh, NY) system, described in detail elsewhere (Geiger et al., 2003), was used to generate a series of four cAMP waves that exhibited the concentration range, average periodicity and symmetry of natural waves (Tomchik and Devreotes, 1981).

To assess mutant cell behavior in wild-type aggregation territories, *pten*$^-$ cells were labeled with DiI (Molecular Probes, Eugene, OR) and mixed with majority unlabeled parental AX2 cells as previously described (Wessels et al., 2004). Transmitted and fluorescent images were collected with a Bio-Rad Radiance 2100MP laser scanning confocal microscope (LSCM) (Bio-Rad, Hemel Hampstead, UK). To assess *pten*$^-$ cell behavior in a *pten*$^-$ aggregation territory, only unlabeled mutant cells were plated in submerged cultures.

2D-DIAS

2D-DIAS software was used for computer-assisted 2D analyses as previously described (Soll, 1995; Soll and Voss, 1998; Wessels et al., 2006). In brief, cells were imaged through a bright-field 25× objective (Falk et al., 2003; Zhang et al., 2003; Heid et al., 2004). Movies were acquired with iStop Motion, exported into QuickTime format and then imported into DIAS. Motility parameters were computed from the centroid positions and dynamic morphology parameters from contours of the replacement images (Soll, 1995; Soll and Voss, 1998; Soll et al., 2000).

3D-DIAS

Cells were optically sectioned and reconstructed using 3D-DIAS software as previously described (Zhang et al., 2003; Wessels et al., 1998; Wessels et al., 2006). In brief, 60 optical sections were collected of live, crawling cells in a 2-second period using DIC optics in a process that was repeated every 5 seconds. The image was captured at 30 frames per second using iMovie software and an analog to digital converter. The resulting iMovie was compressed into the DIAS format. 3D-DIAS software in a newly developed JAVA-based DIAS 4.0 platform automatically outlined the perimeter of the in-focus portion of the image in each optical section using a pixel complexity algorithm (Soll and Voss, 1998; Heid et al., 2005). The distal nonparticulate zones of pseudopodial regions and nuclei were manually outlined in the in-focus portions of each optical section to generate a faceted 3D reconstruction.

Western analysis of myosin II

The protocol for western analysis of myosin II in *pten*$^-$ cells has been described in detail elsewhere (Heid et al., 2004). Briefly, protein concentrations were determined by the method of Bradford (Bradford, 1976). Protein extracts were subjected to SDS-polyacrylamide gel electrophoresis (Laemmli, 1970), then transferred to a PVDF membrane (Immobilon-P, Millipore Corporation, Bedford, MA) using a Trans-Blot semi-dry electrophoretic transfer cell (Bio-Rad, Hercules, CA) and a single buffer system. The membranes were blocked and incubated with rabbit anti-myosin II antibody (generous gifts from Arturo DeLozanne (University of Texas, Austin, TX and Margaret Clarke, Oklahoma Medical Research Foundation, Oklahoma City, OK). The primary antibody was detected using HRP-labeled goat anti-rabbit IgG (Promega, Madison, WI), developed with Super Signal West Pico Chemiluminescent Substrate (Pierce, Rockford, IL) and exposed to X-ray film (Eastman Kodak, Rochester, NY).

Immunostaining of actin and myosin II

For F-actin identification in cells migrating in buffer or in the front of the third temporal wave of cAMP, cells were inoculated into a Sykes-Moore chamber and stained according to methods previously described (Wessels et al., 1989), with minor modifications. In brief, after 5 minutes of perfusion with buffer or midway in the front of the third temporal wave, fixative, consisting of 1% glutaraldehyde, 0.1% Triton X-100 in General Buffer (GB) (Wessels et al., 1989) was rapidly introduced into the Sykes-Moore chamber. After 5 minutes, cells were washed three times with GB containing 1 mg/ml $NaBH_4$ to quench autofluorescence, rinsed once in TBS and stained for 45 minutes with Rhodamine-conjugated phalloidin (Molecular Probes Inc., Eugene, OR) in TBS containing 1% BSA. Coverslips were then rinsed in TBS containing 1% BSA and 0.02% saponin.

For myosin II staining, cells were fixed for 5 minutes in a solution containing 4% paraformaldehyde, 0.05% glutaraldehyde and 0.1% saponin in a phosphate-buffered solution (PBS: 2.7 mM KCl, 1.5 mM KH_2PO4, 8.0 mM Na_2HPO_4). Cells were then rinsed three times in PBS with 1 mg/ml $NaBH_4$ and once with PBS alone, blocked for 45 minutes at 37°C with 10% goat serum in PBS and then rinsed three times in PBS. Cells were then stained with rabbit anti-myosin II antibody (Burns et al., 1995) diluted 1:1000 in 10% goat serum in PBS for 45 minutes at 37°C. Following extensive PBS washes, coverslips were counterstained with Alexa Fluor 488-conjugated goat anti-rabbit IgG (Invitrogen, Inc.) diluted 1:1000 in PBS.

Fluorescence analysis

Cells stained for F-actin or myosin II were mounted in Mowiol (Calbiochem) and imaged with a Bio-Rad Radiance 2100MP laser scanning confocal microscope (LSCM) as previously described (Heid et al., 2004) using procedures designed to obtain comparable measures of the intensity of staining across the cell body (Wessels et al., 2004).

Parental AX2 cells expressing GFP-PTEN were imaged by LSCM, using a 60× plan apochromat water immersion objective (NA 1.2) according to methods previously described (Wessels et al., 2006). A time series of crawling cells was collected at 5-second intervals in an xy time series at a scan rate of 166 lines per second. Line profiles of grayscale intensity were obtained as described above and elsewhere in detail (Wessels et al., 2004; Wessels et al., 2006).

The authors are indebted to Peter Devreotes of Johns Hopkins University for supplying the *pten*$^-$ and *pten*$^-$/PTEN strains, and the *Dictyostelium* Stock Center at Columbia University for supplying the PTEN-GFP construct. This work was funded by National Institutes of Health grant HD-18577 from the Institute of Child Health and Human Development, and the Developmental Studies Hybridoma Bank (DSHB) at Iowa, a national resource. The authors are indebted to Julie Collins for help in assembling the manuscript.

References

Alexander, S., Sydow, L., Wessels, D. and Soll, D. R. (1992). Discoidin proteins of *Dictyostelium* are necessary for normal cytoskeletal organization and cellular morphology during aggregation. *Differentiation* **41**, 149-161.

Andrew, N. and Insall, R. (2007). Chemotaxis in shallow gradients is mediated independently of PtdIns 3-kinase by biased choices between random protrusions. *Nat. Cell Biol.* **9**, 193-200.

Bosgraaf, L., Russcher, H., Smith, J., Wessels, D., Soll, D. and Van Haastert, P. (2002). A novel cGMP signalling pathway mediating myosin phosphorylation and chemotaxis in *Dictyostelium. EMBO J.* **2**, 4560-4570.

Bosgraaf, L., Waijer, A., Engel, R., Visser, A., Wessels, D., Soll, D. R. and Van Hasstert, P. J. M. (2005). RasGEF-containing proteins GbpC and GbpD have differential effects on cell polarity and chemotaxis in *Dictyostelium*. *J. Cell Sci.* **118**, 2225-2237.

Bradford, M. M. (1976). A rapid sensitive method for the quantization of microgram quantities of protein utilizing the principle of protein-dye binding. *Anal. Biochem.* **72**, 248-254.

Buczynski, G., Grove, B., Nomura, A., Kleve, M., Bush, J., Firtel, R. A. and Cardelli, J. (1997). Inactivation of two *Dictyostelium discoideum* genes, *DdPIK1* and *DdPIK2*, encoding proteins related to mammalian phosphatidylinositide 3-kinases, results in defects in endocytosis, lysosome to postlysosome transport, and actin cytoskeleton organization. *J. Cell Biol.* **136**, 1271-1286.

Burns, C. G., Reedy, M., Heuser, J. and De Lozanne, A. (1995). Expression of light meromyosin in *Dictyostelium* blocks normal myosin II function. *J. Cell Biol.* **130**, 605-612.

Chen, L., Janetopoulos, S. C., Huang, Y. E., Iijima, M., Borleis, J. and Devreotes, P. N. (2003). Two phases of actin polymerization display different dependencies on $PI(3,4,5)P_3$ accumulation and have unique roles during chemotaxis. *Mol. Biol. Cell* **14**, 5028-5037.

Cho, W. and Stahelin, R. (2006). Membrane binding and subcellular targeting of C2 domains. *Biochim. Biophys. Acta* **8**, 838-849.
Cocucci, S. and Sussman, M. (1970). RNA in cytoplasmic and nuclear fractions of cellular slime mold amebas. *J. Cell Biol*. **45**, 399-407.
Condeelis, J., Hall, A., Bresnick, A., Warren, V., Hock, R., Bennett, H. and Ogihara, S. (1988). Actin polymerization and pseudopod extension during amoeboid chemotaxis. *Cell Motil. Cytoskeleton* **10**, 77-90.
Cox, D., Condeelis, J., Wessels, D., Soll, D. R., Kern, H. and Knecht, D. (1992). Targeted disruption of the ABP-120 gene leads to cells with altered motility. *J. Cell Biol.* **116**, 943-955.
Cox, D., Wessels, D., Soll, D. R., Hartwig, J. and Condeelis, J. (1996). Re-expression of ABP-120 rescues cytoskeletal, motility, and phagocytosis defects of ABP-120^{-} *Dictyostelium* mutants. *Mol. Biol. Cell* **7**, 803-823.
Dai, J., Ting-Beall, H., Hochmuth, R., Sheetz, M. and Titus, M. (1999). Myosin I contributes to the generation of resting cortical tension. *Biophys. J*. **77**, 1168-1176.
Devreotes, P. and Janetopoulos, C. (2003). Eukaryotic chemotaxis: distinctions between directional sensing and polarization. *J. Biol. Chem.* **278**, 20445-20448.
Dharmwardhane, S., Warren, V., Hall, A. and Condeelis, J. (1989). Changes in the association of actin-binding proteins with the actin cytoskeleton during chemotactic stimulation of *Dictyostelium discoideum*. *Cell Motil. Cytoskeleton* **13**, 57-63.
Dormann, D., Weijer, G., Dowler, S. and Weijer, C. J. (2004). In vivo analysis of 3-phosphoinositide dynamics during *Dictyostelium* phagocytosis and chemotaxis. *J. Cell Sci.* **117**, 6497-6509.
Egelhoff, T., Lee, R. and Spudich, J. (1993). *Dictyostelium* myosin heavy chain phosphorylation sites regulate myosin filament assembly and localization in vivo. *Cell* **75**, 363-371.
Egelhoff, T. T., Nasmyth, T. V. and Brozovich, F. V. (1996). Myosin-based cortical tension in *Dictyostelium* resolved into heavy and light chain-regulated components. *J. Muscle Res. Cell Motil.* **17**, 269-274.
Escalante, R., Wessels, D., Soll, D. R. and Loomis, W. F. (1997). Chemotaxis to cAMP and slug migration in *Dictyostelium* both depend on migA, a BTB protein. *Mol. Biol. Cell* **8**, 1763-1765.
Falk, D. L., Wessels, D., Jenkins, L., Pham, T., Kuhl, S., Titus, M. A. and Soll, D. R. (2003). Shared, unique and redundant functions of three members of the class I myosins (MyoA, MyoB and MyoF) in motility and chemotaxis in *Dictyostelium*. *J. Cell Sci.* **116**, 3985-3999.
Ferguson, G., Milne, L., Kulkarni, S., Sasaki, T., Walker, S., Andrews, S., Crabbe, T., Finan, P., Jones, G., Jackson, S. et al. (2007). PI(3)Kγ has an important context-dependent role in neutrophil chemokinesis. *Nat. Cell Biol*. **9**, 86-91.
Franca-Koh, J., Kamimura, Y. and Devreotes, P. N. (2007). Leading edge research: Ptd(Ins3,4,5)P_3 and directed migration. *Nat. Cell Biol.* **9**, 15-17.
Funamoto, S., Milan, K., Meili, R. and Firtel, R. A. (2001). Role of phosphatidylinositol 3′ kinase and a downstream pleckstrin homology domain-containing protein in controlling chemotaxis in *Dictyostelium*. *J. Cell Biol*. **153**, 795-810.
Funamoto, S., Meili, R., Lee, S., Parry, L. and Firtel, R. A. (2002). Spatial and temporal regulation of 3-phosphoinositides by PI 3-kinase and PTEN mediates chemotaxis. *Cell* **109**, 611-623.
Futrelle, R. R., Trant, J. and McKee, W. G. (1981). Cell behavior in *Dictyostelium discoideum* preaggregation response to localized cAMP pulses. *J. Cell Biol.* **92**, 807-821.
Geiger, J., Wessels, D. and Soll, D. R. (2003). Human PMNs respond to temporal waves of chemoattractant like *Dictyostelium*. *Cell Motil. Cytoskeleton* **56**, 27-44.
Hall, A. L., Schlein, A. and Condeelis, J. (1988). Relationship of pseudopod extension to chemotactic hormone-induced actin polymerization in amoeboid cells. *J. Cell. Biochem.* **37**, 285-299.
Haugh, J., Codazzi, F., Teruel, M. and Meyer, T. (2000). Spatial sensing in fibroblasts mediated by 3′phosphoinositides. *J. Cell Biol.* **151**, 1269-1280.
Heid, P., Voss, E. and Soll, D. R. (2002). 3D-DIASemb: a computer-assisted system for reconstruction and motion analyzing in 4D every cell and nucleus in a developing embryo. *Dev. Biol*. **245**, 329-347.
Heid, P. J., Wessels, D., Daniels, K. J., Zhang, H. and Soll, D. R. (2004). The role of myosin heavy chain phosphorylation in *Dictyostelium* motility, chemotaxis and F-actin localization. *J. Cell Sci.* **117**, 4819-4835.
Heid, P., Geiger, J., Wessels, D., Voss, E. and Soll, D. R. (2005). Computer-assisted analysis of filopod formation and the role of myosin II heavy chain phosphorylation in *Dictyostelium*. *J. Cell Sci*. **118**, 2225-2237.
Hoeller, O. and Kay, R. R. (2007). Chemotaxis in the absence of PIP3 gradients. *Curr. Biol.* **17**, 813-817.
Huang, Y., Iijima, M., Parent, C., Funamoto, S., Firtel, R. and Devreotes, P. (2003). Receptor-mediated regulation of PI3Ks confines PI(3,4,5)P3 to the leading edge of chemotaxing cells. *Mol. Biol. Cell* **14**, 1913-1922.
Iijima, M. and Devreotes, P. N. (2002). Tumor suppressor PTEN mediates sensing of chemoattractant gradients. *Cell* **109**, 599-610.
Iijima, M., Huang, Y. E., Luo, H. R., Vazquez, F. and Devreotes, P. N. (2004). Novel mechanism of PTEN regulation by its phosphatidylinositol 4,5-biophosphate binding motif is critical for chemotaxis. *J. Biol. Chem.* **279**, 16606-16613.
Janetopoulos, C., Ma, L., Devreotes, P. N. and Iglesias, P. A. (2004). Chemoattractant-induced phosphatidylinositol 3,4,5-triphosphate accumulation is spatially amplified and adapts, independent of the actin cytoskeleton. *Proc. Natl. Acad. Sci. USA* **101**, 8951-8956.
Kumar, A., Wessels, D., Daniels, K., Alexander, H., Alexander, S. and Soll, D. R. (2004). Sphingosine-1-phosphate plays a role in the suppression of lateral pseudopod formation during *Dictyostelium discoideum* cell migration and chemotaxis. *Cell Motil. Cytoskeleton* **59**, 227-241.
Lacalle, R., Gómez-Moutón, C., Barber, D., Jiménez-Baranda, S., Mira, E., Martínez-A., C., Carrera, A. and Mañes, S. (2004). PTEN regulates motility but not directionality during leukocyte chemotaxis. *J. Cell Sci.* **117**, 6207-6215.
Laemmli, U. K. (1970). Cleavage of structural proteins during the assembly of the head of the bacteriophage T4. *Nature* **227**, 592-596.
Laevsky, G. and Knecht, D. (2003). Cross-linking of actin filaments by myosin II is a major contributor to cortical integrity and cell motility in restrictive environments. *J. Cell Sci*. **116**, 3761-3770.
Lee, J., Yang, H., Georgescu, M., Di Cristofano, A., Maehama, T., Shi, Y., Dixon, J., Pandolfi, P. and Pavletich, N. (1999). Crystal structure of the PTEN tumor suppressor: implications for its phosphoinositide phosphatase activity and membrane association. *Cell* **99**, 323-334.
Lee, R., Egelhoff, T. and Spudich, J. (1994). Molecular genetic truncation analysis of filament assembly and phosphorylation domains of *Dictyostelium* myosin heavy chain. *J. Cell Sci.* **107**, 2875-2886.
Levi, S., Polyakov, M. and Egelhoff, T. (2002). Myosin II dynamics in *Dictyostelium*: determinants for filament assembly and translocation to the cell cortex during chemoattractant responses. *Cell Motil. Cytoskeleton* **53**, 177-188.
Li, J., Yen, D., Liaw, D. and Podsypanina, K. (1997). *PTEN*, a putative protein tyrosine phosphatase gene mutated in human brain, breast and prostate cancer. *Science* **275**, 1943-1947.
Lück-Veilmetter, D., Schleicher, M., Grabatin, B., Wippler, J. and Gerisch, G. (1990). Replacement of threonine residues by serine and alanine in a phosphorylatable heavy chain fragment of *Dictyostelium* myosin II. *FEBS Letts*. **269**, 239-243.
McRobbie, S. J. and Newell, P. C. (1983). Changes in actin associated with the cytoskeleton following chemotactic stimulation of *Dictyostelium discoideum*. *Biochem. Biophys. Res. Commun.* **115**, 351-359.
Meili, R., Ellsworth, C., Lee, S., Reddy, T., Ma, H. and Firtel, R. A. (1999). Chemoattractant-mediated transient activation and membrane localization of Akt/PKB is required for efficient chemotaxis to cAMP in *Dictyostelium*. *EMBO J.* **18**, 2092-2105.
Moores, S. and Spudich, J. (1996). Myosin dynamics in live *Dictyostelium* cells. *Proc. Natl. Acad. Sci. USA* **93**, 443-446.
Nishio, M., Watanabe, K., Sasaki, J., Taya, C., Iizuka, R., Balla, T., Yamazaki, M., Watanabe, H., Itoh, R., Kurodo, S. et al. (2007). Control of cell polarity and motility by the PtdIns(3,4,5)P3 phosphatase SHIP1. *Nat. Cell Biol.* **9**, 36-44.
Parent, C. and Devreotes, P. (1999). A cell's sense of direction. *Science* **284**, 765-770.
Pasternak, C., Spudich, J. and Elson, E. (1989). Capping of surface receptors and concomitant cortical tension are generated by conventional myosin. *Nature* **341**, 549-551.
Peters, D. J. M., Knecht, D. A., Loomis, W. F., Lozanne, A. D., Spudich, J. A. and Van Haastert, P. J. M. (1988). Signal transduction, chemotaxis and cell aggregation in *Dictyostelium discoideum* cells without myosin heavy chain. *Dev. Biol.* **128**, 158-163.
Postma, M., Roelofs, J., Goedhart, J., Gadella, T. W., Visser, A. J. and Van Haastert, P. (2003). Uniform cAMP stimulation of *Dictyostelium* cells induces localized patches of signal transduction and pseudopodia. *Mol. Biol. Cell* **14**, 5019-5027.
Postma, M., Roelofs, J., Goedhart, J., Loovers, H. M., Visser, A. J. and Van Haastert, P. J. M. (2004). Sensitization of *Dictyostelium* chemotaxis by phosphoinositide-3-kinase-mediated self-organizing signalling patches. *J. Cell Sci*. **117**, 2925-2935.
Servant, G., Weiner, O., Herzmark, P., Balla, T., Sedat. J. and Bourne, H. (2000). Polarization of chemoattractant receptor signaling during neutrophil chemotaxis. *Science* **287**, 1037-1040.
Sheldon, E. and Knecht, D. (1996). *Dictyostelium* cell shape generation requires myosin II. *Cell Motil. Cytoskeleton* **75**, 218-226.
Shutt, D., Wessels, D., Wagenknecht, K., Chandrasekhar, A., Hitt, A., Luna, E. and Soll, D. R. (1995). Ponticulin plays a role in the positional stabilization of pseudopods. *J. Cell Biol*. **131**, 1495-1506.
Shutt, D. C., Jenkins, L. M., Carolan, E., Stapleton, J., Daniels, K., Kennedy, R. and Soll, D. R. (1998). T cell syncytia induced by HIV release T cell chemoattractants: demonstration with a newly developed single cell chemotaxis chamber. *J. Cell Sci*. **111**, 99-109.
Soll, D. R. (1979). Timers in developing systems. *Science* **203**, 841-849.
Soll, D. R. (1995). The use of computers in understanding how animal cells crawl. *Int. Rev. Cytol*. **163**, 43-104.
Soll, D. R. and Voss, E. (1998). Two and three dimensional computer systems for analyzing how cells crawl. In *Motion Analysis of Living Cells* (ed. D. R. Soll and D. Wessels), pp. 25-52. New York: John Wiley.
Soll, D., Voss, E., Johnson, O. and Wessels, D. (2000). Three dimensional reconstruction and motion analysis of living crawling cells. *Scanning* **22**, 249-257.
Soll, D. R., Wessels, D., Zhang, H. and Heid, P. (2002). A contextual framework for interpreting the roles of proteins in motility and chemotaxis in *Dictyostelium discoideum.* Special *Dictyostelium* issue. *J. Musc. Res. Cell Motil*. **23**, 659-672.
Sonnemann, J., Knoll, G. and Schlatterer, C. (1997). cAMP-induced changes in the cytosolic free Ca^{2+} concentration in *Dictyostelium discoideum* are light sensitive. *Cell Calcium* **22**, 65-74.
Spudich, J. (1989). In pursuit of myosin function. *Cell Regul*. **1**, 1-11.
Steck, P., Pershouse, M., Jasser, S., Yung, A., Lin, H., Ligon, A., Langford, L., Baumgard, M., Hattier, T., Dairs, T. et al. (1997). Identification of a candidate tumour suppressor gene, *MMAC1*, at chromosome 10q23.3 that is mutated in multiple advanced cancers. *Nat. Genet*. **15**, 356-362.
Stepanovic, V., Wessels, D., Daniels, K., Loomis, W. F. and Soll, D. R. (2005). Intracellular role of adenylyl cyclase in regulation of lateral pseudopod formation during *Dictyostelium* chemotaxis. *Eukaryotic Cell* **4**, 775-786.

Subramanian, K., Jia, Y., Zhu, D., Simms, B., Jo, H., Hattori, H., You, J., Mizgerd, J. and Luo, H. (2007). Tumor suppressor PTEN is a physiological suppressor of chemoattractant-mediated neutrophil functions. *Blood* **109**, 4028-4037.

Sulis, M. and Parsons, R. (2003). PTEN: from pathology to biology. *Trends Cell Biol.* **13**, 478-483.

Titus, M., Wessels, D., Spudich, J. and Soll, D. R. (1993). The unconventional myosin encoded by the *myoA* gene plays a role in *Dictyostelium* motility. *Mol. Biol. Cell* **4**, 233-246.

Tomchik, K. J. and Devreotes, P. N. (1981). Adenosine 3′,5′-monophosphate waves in *Dictyostelium discoideum*: a demonstration by isotope dilution-fluorography. *Science* **212**, 443-446.

Varnum, B. and Soll, D. R. (1984). Effect of cAMP on single cell motility in *Dictyostelium*. *J. Cell Biol*. **99**, 1151-1155.

Varnum, B., Edwards, K. B. and Soll, D. R. (1985). *Dictyostelium* amoebae alter motility differently in response to increasing versus decreasing temporal gradients of cAMP. *J. Cell Biol.* **101**, 1-5.

Varnum, B., Edwards, K. and Soll, D. R. (1986). The developmental regulation of single cell motility in *Dictyostelium discoideum*. *Dev. Biol.* **113**, 218-227.

Varnum-Finney, B., Edwards, K., Voss, E. and Soll, D. R. (1987a). Amoebae of *Dictyostelium discoideum* respond to an increasing temporal gradient of the chemoattractant cAMP with a reduced frequency of turning: evidence for a temporal mechanism in amoeboid chemotaxis. *Cell Motil. Cytoskeleton* **8**, 7-17.

Varnum-Finney, B., Voss, E. and Soll, D. R. (1987b). Frequency and orientation of pseudopod formation of *Dictyostelium discoideum* amoebae chemotaxing in a spatial gradient: Further evidence for a temporal mechanism. *Cell Motil. Cytoskeleton* **8**, 18-26.

Varnum-Finney, B., Schroeder, N. A. and Soll, D. R. (1988). Adaptation in the motility response to cAMP in *Dictyostelium discoideum*. *Cell Motil. Cytoskeleton* **9**, 9-16.

Vazquez, F., Matsuoka, S., Sellers, W., Yanagida, T., Ueda, M. and Devreotes, P. (2006). Tumor suppressor PTEN acts through dynamic interaction with the plasma membrane. *Proc Natl. Acad. Sci. USA* **103**, 3633-3638.

Wessels, D. and Soll, D. R. (1990). Myosin II heavy chain null mutant of *Dictyostelium* exhibits defective intracellular particle movement. *J. Cell Biol*. **111**, 1137-1148.

Wessels, D. and Soll, D. R. (1998). Computer-assisted characterization of the behavioral defects of cytoskeletal mutants of *Dictyostelium discoideum*. In *Motion Analysis of Living Cells* (ed. D. R. Soll and D. Wessels), pp. 101-140. New York: John Wiley.

Wessels, D., Soll, D. R., Knecht, D., Loomis, W. F., De Lozanne, A. and Spudich, J. (1988). Cell Motility and chemotaxis in *Dictyostelium* amoebae lacking myosin heavy chain. *Dev. Biol.* **128**, 164-177.

Wessels, D., Schroeder, N., Voss, E., Hall, A., Condeelis, J. and Soll, D. R. (1989). cAMP-mediated inhibition of intracellular particle movement and actin reorganization in *Dictyostelium*. *J. Cell Biol*. **109**, 2841-2851.

Wessels, D., Murray, J. and Soll, D. R. (1992). Behavior of *Dictyostelium* amoebae is regulated primarily by the temporal dynamic of the natural cAMP wave. *Cell Motil. Cytoskeleton* **23**, 145-156.

Wessels, D., Titus, M. and Soll, D. R. (1996). A *Dictyostelium* myosin I plays a crucial role in regulating the frequency of pseudopods formed on the substratum. *Cell Motil. Cytoskeleton* **33**, 64-79.

Wessels, D., Voss, E., Von Bergen, N., Burns, R., Stites, J. and Soll, D. R. (1998). A computer-assisted system for reconstructing and interpreting the dynamic three-dimensional relationships of the outer surface, nucleus and pseudopods of crawling cells. *Cell Motil. Cytoskeleton* **41**, 225-246.

Wessels, D., Reynolds, J., Johnson, O., Voss, E., Burns, R., Daniels, K., Garrard, E., O'Hallaran, T. and Soll, D. R. (2000a). Clathrin plays a novel role in the regulation of cell polarity, pseudopod formation, uropod stability and motility in *Dictyostelium. J. Cell Sci*. **113**, 26-36.

Wessels, D., Zhang, H., Reynolds, J., Daniels, K., Heid, P., Liu, S., Kuspa, A., Shaulsky, G., Loomis, W. F. and Soll, D. R. (2000b). The internal phosphodiesterase *RegA* is essential for the suppression of lateral pseudopods during *Dictyostelium* chemotaxis. *Mol. Biol. Cell* **11**, 2803-2820.

Wessels, D., Brincks, R., Kuhl, S., Stepanovic, S., Daniels, K. J., Weeks, G., Lim, C. J., Fuller, D., Loomis, W. F. and Soll, D. R. (2004). RasC plays a selective role in the transduction of temporal gradient information in the cAMP wave of *Dictyostelium. Eukaryotic Cell* **3**, 646-662.

Wessels, D., Kuhl, S. and Soll, D. R. (2006). Application of 2D and 3D DIAS to motion analysis of live cells in transmission and confocal microscopy. *Methods Mol. Biol*. **346**, 261-279.

Yumura, S. and Fukui, Y. (1985). Reversible cAMP-dependent change in distribution of myosin thick filaments in *Dictyostelium*. *Nature* **314**, 194-196.

Yumura, S. and Uyeda, T. (1997). Myosin II can be localized to the cleavage furrow and to the posterior region of *Dictyostelium* amoebae without control by phosphorylation of myosin heavy and light chains. *Cell Motil. Cytoskeleton* **36**, 313-322.

Zhang, H., Wessels, D., Fey, P., Daniels, K., Chisholm, R. and Soll, D. R. (2002). Phosphorylation of the myosin regulatory light chain plays a role in cell motility and polarity during *Dictyostelium* chemotaxis. *J. Cell Sci.* **115**, 1733-1747.

Zhang, H., Heid, P., Wessels, D., Daniels, K., Pham, T., Loomis, W. F. and Soll, D. R. (2003). Constitutively active protein kinase A disrupts motility and chemotaxis in *Dictyostelium discoideum. Eukaryotic Cell* **2**, 62-75.

Zhou, K., Pandol, S., Bokoch, G. and Traynor-Kaplan, A. (1998). Disruption of *Dictyostelium* PI3K genes reduces [32^{P}]phosphatidylinositol 3,4 bisphosphate and [32^{P}]phosphatidylinositol trisphosphate levels, alters F-actin distribution and impairs pinocytosis. *J. Cell Sci.* **111**, 283-204.

Zigmond, S. H. (1977). The ability of polymorphonuclear leukocytes to orient in gradients of chemotaxis factors. *J. Cell Biol.* **75**, 606-616.